Abstract

YOHANNAN, JOSHUA CHARLES

INVESTIGATION OF THE PHOTOPHYSICAL AND ELECTROCHEMICAL PROPERTIES OF DENDRIMERS BASED ON A $[Re_6Se_8]^{2+}$ CORE.

(Under the direction of Dr. Christopher B. Gorman)

Dendritic molecules have demonstrated the ability to encapsulate metal cluster cores and shield them from an external environment. The ability to shield the metal cluster core results in altering of some of the measurable properties of that metal cluster.

The photophysical and electrochemical data on an octahedral rhenium-selenide cluster dendrimer was examined. This rhenium-selenide metal cluster was chosen as the dendrimer core because previously characterized rhenium-selenide metal clusters have been shown to luminescence and possess accessible electrochemistry. For these investigations a dendron that has previously been used for encapsulation and still allowed access to an electroactive core were used. The focal point of these dendrons was slightly modified in order to attach them to the rhenium-selenide core. Photophysical and electrochemical investigations were completed on generations zero through two of these dendrimer.

INVESTIGATION OF THE PHOTOPHYSICAL AND ELECTROCHEMICAL PROPERTIES OF DENDRIMERS BASED ON A $[Re_6Se_8]^{2+}$ CORE

by

JOSHUA CHARLES YOHANNAN

A thesis submitted to the Graduate Faculty of
North **C**arolina **S**tate **U**niversity
in partial fulfillment of the requirements for the
Degree of Master of Science

CHEMISTRY

Raleigh, North Carolina
2003

APPROVED BY:

_____
Christopher B. Gorman
Chair of Advisory Committee

_____ _____
Daniel Feldheim Jim Martin

Biography

Joshua C. Yohannan was born March 13th, 1978 in Geneva, New York. Josh's parents, Robert and Deborah Yohannan helped guide him through the Wallingford-Swarthmore school district for grades 2 through 12. Josh graduated from Strath Haven high school in 1996.

Josh went on to attended Vassar College in Poughkeepsie, New York. At Vassar Josh earned a Bachelor of Arts in chemistry and economics. Josh successfully completed the thesis requirements for the chemistry department and was a member of the economics' honor society, Omicron Delta Epsilon. Josh balanced his academics with lacrosse and finished his four-year career as the top goalie in Vassar history.

Having decided early in his academic career that he wanted to pursue a higher degree, Josh continued his work in chemistry at North Carolina State University. He completed his work under the guidance of Dr. Chris Gorman.

Table of Contents

List of Figures iv
List of Tables v
Chapter 1 : Background Information 1
Introduction 1
Dendrimers 2
Electrochemical Properties 14
Photophysical properties 27
Molecule 29
Energy Transfer 31
Rhenium-Selenide Core 34
Cluster 41
Rhenium-selenide core dendrimers 43
Summary 46
Chapter 1 References 48
Chapter 2 : Synthesis 52
Introduction 52
Core Synthesis 52
Dendron Synthesis 57
Ligand Exchange 58
Conclusion 64
Experimental 65
Chapter 2 References 70
Chapter 3 : Photophysical Investigations 71
Introduction 71
Results and Discussion 72
UV-Vis 72
Quantum Yield 74
Energy Transfer 77
Experimental 82
Chapter 3 References 87
Chapter 4 : Electrochemical Investigation 89
Introduction 89
Results and Discussion 89
CV 89
Chronoamperometry 93
OYSW 94
Experimental 96
Chapter 4 References 99

List of Figures

Figure 1.1: Basic dendron structure 4
Figure 1.2: Cartoon depiction of a possible problem with Abruña's dendrimers and electrochemical determination of diffusion coefficients 11
Figure 1.3: Cartoon depiction of encapsulation affecting the distance that an electron must travel 15
Figure 1.4: First generation rigid and flexible dendrons 17
Figure 1.5: Snapshot of low-energy conformations determined by computer simulations showing the offset cores of fourth generation flexible (top) and rigid (bottom) dendrimers 18
Figure 1.6: Energy level diagrams explaining the difference between dendrimers where a change in redox potential is observed and dendrimers that exhibit no change 20
Figure 1.7: Heterogeneous electron rate transfer constants for flexible and rigid iron-sulfur core dendrimers 25
Figure 1.8: Heterogeneous electron transfer rates as a function of molecular radius for flexible and rigid iron-sulfur core dendrimers 26
Figure 1.9: Cartoon depiction of effective electron transfer distance differences between extended and backfolded iron-sulfur core dendrimers 27
Figure 1.10: Energy level diagram depicting intramolecular exciton transfer 31
Figure 1.11: Octahedral rhenium-selenide cluster 35
Figure 1.12: Dimensional reduction 36
Figure 1.13: Energy level diagrams for $[Mo_6S_8]^{4-}$ cores 40
Figure 1.14: Zheng's dendron structures 44
Figure 1.15: Zheng's dendron designed with terminal rhenium-selenide clusters 45
Figure 2.1: Three-step synthesis of rhenium-selenide core 52
Figure 2.2: Oven Diagram 54
Figure 2.3: ^1H NMR of $[Re_6Se_8(CH_3CN)_6](SbF_6)_2$ 57
Figure 2.4: Dendron synthesis and structures 58
Figure 2.5: Ligand exchange conditions 59
Figure 2.6: G0 ^1H NMR 61
Figure 2.7: G1 ^1H NMR 62
Figure 2.8: G2 ^1H NMR 63
Figure 3.1: UV-Vis absorbance of G1 dendrimer in methylene chloride 72
Figure 3.2: Extinction Coefficients for Various Concentrations 73
Figure 3.3: Emission spectra of a freshly prepared solution vs. a day-old solution 76
Figure 3.4: G1 dendrimer absorbance and G1 dendron emission 78
Figure 3.5: Emission spectra of G2 dendron and G2 dendrimer excited at 276nm 79
Figure 3.6: Emission spectra of G2 dendrimer when excited at 436nm vs. when excited at 276nm 81
Figure 4.1: G0 dendrimer acting as a freely diffusing molecule 91
Figure 4.2: Cyclic voltammery of $[Re_6Se_8(CH_3CN)_6]^{2+}$, $[Re_6Se_8(G0)_6]^{2+}$, and $[Re_6Se_8(G1)_6]^{2+}$ in propylene carbonate, scan rates were 100mV/sec 92
Figure 4.3: Cyclic voltammetry of $[Re_6Se_8(CH_3CN)_6]^{2+}$ and $[Re_6Se_8(G0)_6]^{2+}$ in dimethylformamide with 100mV/sec scan rate 93
Figure 4.4: Oysteryoung squarewave voltammetry of $[Re_6Se_8(CH_3CN)_6]^{2+}$ and $[Re_6Se_8(G0)_6]^{2+}$ in propylene carbonate 95

List of Tables

Table 1.1: Diffusion coefficients of PAMAM dendrimers (cm^2/sec) 9
Table 1.2: Diffusion coefficients and hydrodynamic radii for constituational isomers determined by PFGSE-NMR 13
Table 1.3: Redox potentials of iron porphyrin core dendrimers in various solvents 22
Table 1.4: redox potentials of ferrocene core dendrimers 23
Table 1.5: Redox potentials of iron-sulfur core constitutional isomer dendrimers 24
Table 1.6: Quantum yield and emission lifetimes of ruthenium core dendrimers 29
Table 1.7: Energy transfer quantum yield values for perylene-terminated dendrimers ... 33
Table 1.8: Mean bond lengths (Å) and bond angles (degrees) of rhenium-selenide clusters 36
Table 1.9: Selected photophysical properties of rhenium-chalcogen molecules 41
Table 3.1: Quantum yield values of rhenium-selenide core dendrimers 74
Table 4.1: Electrochemical values of $[Re_6Se_8(CH_3CN)_6]^{2+}$ and $[Re_6Se_8(G0)_6]^{2+}$ 92

Chapter 1 : Background Information

Introduction

Dendrimers have drawn much interest with the development of organic light emitting devices (oLEDs)[1-3]. Simple organic light emitting devices consist of a cathode, light emitting layer, and an anode. Dendrimers are considered a good material for the emitting layer because they have exhibited redox behavior and many dendrimers are luminescent[4-15]. This interest has led to the investigation of many different dendrimer cores depending on the physical properties desired. Previous investigations have demonstrated that the photophysical and electrochemical properties of the dendrimer core can be significantly tailored by the architecture of the dendrimeric ligands. Dendrimeric ligands have been shown to enhance the quantum yield an emission lifetimes when compared to unmodified cores. These increases are due to the inability of small molecules to quench the fluorescence. The electrochemical properties of dendrimers are also beneficial for oLEDs. Dendrimers increase the distance between a redox active core and an electrode causing a decrease in redox kinetics. This decrease in electron transfer kinetics to the electrode allows a greater probability for electron-hole recombination within the emitting layer. Rhenium-selenide clusters are attractive as a photoactive dendrimer core because of the redox activity of the cluster and its high luminescent quantum yields and emission lifetimes. (reference) However, previous investigations have shown rhenium-selenide core dendrimers to exhibit irreversible electrochemical behavior in solution, suggesting that they would be a poor choice for use in oLEDs. (reference) It is anticipated that with ligand modification it should be possible

to create a dendrimer with reversible electrochemistry that will also allow the exploitation of the beneficial luminescent properties of the rhenium-selenide core.

In this thesis the use of poly(benzyl ether) dendrons with a benzonitrile focal point surrounding an octahedral rhenium-selenide core is described. This design offers better redox kinetics than previously synthesized rhenium-selenide core dendrimers and exhibits high quantum yields in solution. The poly(benzyl ether) dendrons used have previously been used for electrochemical studies[9, 16-21] and photophysical studies[4, 11, 22-26]. The benzonitrile was chosen based on previous luminescent studies, where this linkage exhibited high quantum yields and emission lifetimes. The rhenium-selenide core dendrimers synthesized exhibited slow redox kinetics and high quantum yields as expected.

The introductory chapter to this thesis will introduce pertinent background information about dendrimers and the rhenium-selenide core. Chapter 2 will discuss the synthesis of the dendrimer core, dendrons, and the ligand exchange conditions. Many of the synthetic steps have been previously reported, but this chapter will go into more detail and highlight some of the important areas of concern with each step. The 3rd and 4th chapters will discuss the photophysical and electrochemical characterization of zero-, first-, and second-generation dendrimers.

Dendrimers

Dendrimers represent a unique class of molecules that have been shown to possess interesting solution and solid-state characteristics. Dendrimer research began in 1985 with work by Newkome[27] and Tomalia[28] and the hyperbranched molecules have drawn much interest since. Dendrimer research has focused on physical,

photophysical, and electrochemical properties. As the properties have begun to be understood, there have been investigations into possible applications for dendrimers.

The structure of a dendrimer is described as one or more hyperbranched polymeric ligands, referred to as dendrons, radiating from a central core. A basic dendron is shown in **Figure 1.1**. The core may consist of single metal atoms, metal clusters, porphyrins, or polymers. The dendrons consist of organic and/or inorganic components, with specific repeat units. The point of interaction between the core and the dendron is the focal point. The strength and type of interaction between the dendron and the core is controlled through the choice of focal point. Dendrons consist of a controlled number of repeat units. Each repeat unit is attached to a branch point and the number of branch points refers to the dendron generation. Each additional branch point increases the dendron generation by one. At the periphery of the dendron are the terminal groups. These groups are the point of interaction between the dendrimer and the surrounding environment and affect properties such as solubility and diffusion coefficient[5, 7-9, 14, 16-19, 21, 29, 30]. The number of terminal groups will increase based on the design of the dendron. For example, a dendron with two terminal groups per dendron will result in the number of terminal groups doubling with an increase of one generation. The total number of terminal groups for any generation of this dendron may be found using 2^n, where n is the dendron generation.

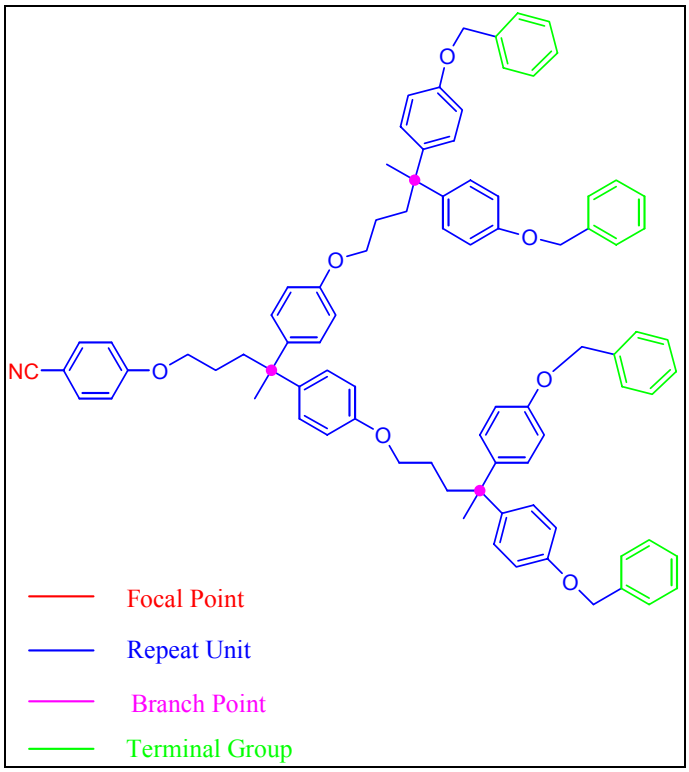


Figure 1.1: Basic dendron structure

The synthesis of dendrimers has been divided into two different schemes, divergent and convergent. Tomalia[28] first developed the scheme for the divergent synthesis in 1985. Divergent synthesis begins at the core and uses an activation/coupling scheme to add repeat units to the core. One repeat unit was added at each coupling step, resulting in an increase of one generation with each coupling step. The main advantage to divergent synthesis is the ability to produce high molecular weight products. The main disadvantage to this approach is the purification steps necessary following each activation and coupling reaction. The other disadvantage to this approach is the possibility of defects within the dendrimer. Because these defects may be small, the separation of pure dendrimer and impure dendrimer may be difficult. These defects may multiply following

each activation/coupling step, causing the polydispersity to be larger then can be achieved through the convergent approach.

In response to the problems associated with the divergent synthesis, Frechet[31] and co-workers developed a new method known as the convergent scheme. Convergent synthesis is defined by the separate synthesis of the core and the dendron followed by ligand exchange to form the dendrimer. Dendrons of increasing generation were synthesized by the same activation and coupling scheme as in the divergent synthesis. One key factor is the need for protection of the focal point during the dendron synthesis. With the focal point protected, or added last, dendrons are synthesized to the desired generation prior to ligand exchange. Convergent synthesis requires purification of the core and dendrons prior to ligand exchange, therefore minimizing the amount of purification necessary following ligand exchange. The main disadvantage to convergent synthesis is the inability to synthesize very high molecular weight dendrimers. Higher generation dendrimers are difficult to synthesize due to the steric hindrance of large dendrons during ligand exchange.

At higher generations dendrimers are believed to adopt a globular shape with the dendrons surrounding the core. The globular shape provides an interior microenvironment where the dendrimer core resides. Design of the repeat unit will determine the properties of this interior environment. The interior of a dendrimer can be designed to be hydrophobic, hydrophilic, polar, or nonpolar depending on the desired application. As previously stated, the terminal groups are the point of interaction between the dendrimer and the outside environment. The terminal groups help determine solubility and also may determine the hydrodynamic radius of the dendrimer in different

solvents[7-9, 16-19, 29, 30]. Kaifer[30] previously designed terminal groups to control the orientation of a dendrimer with respect to an electrode, thereby showing the ability of terminal groups to interact with the external environment.

It is a combination of the structure of the dendrons and their interactions with the surrounding environment that have led to the concept of encapsulation. Encapsulation is the ability of a dendrimer to shield the dendrimer core from an external environment. Encapsulation is observed through a change in the measurable properties of the dendrimer core. Although encapsulation may occur with dendrimer cores lacking measurable properties there is no way to show this phenomenon. The ability to change the intrinsic properties of the dendrimer core is reminiscent of the ability of metalloproteins to modify the intrinsic properties of the protein core.

Encapsulation effects have been studied in many different ways. There are three major core properties that have been investigated: solubility, electrochemical, and photophysical. There have been studies focusing on the effects of increasing dendrimer generations, changing dendritic structures, and comparing dendrimers and their linear analogs.

One area of experimental focus within dendrimer research has been attempts to improve the solubility of insoluble cores. Dendron structure can be modified to have specific regions of hydrophobic and hydrophilic components, resulting in improved solubility in a desired solvent. Most often the desire has been to make dendrimers water-soluble. Fréchet[32] described dendrimers as being unimolecular micelles when discussing the possibility of water solubility. According to this description, the dendrimer would be designed such that the interior of the dendron would be hydrophobic

and the terminal groups would be hydrophilic. This design should result in the hydrophobic interior environment contracting around the core and the hydrophilic terminal groups extending outward making the dendrimer soluble in aqueous solutions. Attempts to synthesize water-soluble dendrimers have included PAMAM dendrons, carboxylic salts, and PEG units.

In order to understand generational and dendron structure effects, dendrimers were studied in solution. Solution studies elucidated how the dendritic architecture affects diffusion coefficients and hydrodynamic radii. Hawker[33] investigated the difference in physical properties between dendrimers and their linear analogues in solution. Polybenzyl-ether dendrons surrounding a porphyrin core were compared to their linear equivalents. The most notable difference was the crystalline nature of the different samples. The dendrimers studied were crystalline only at generations one and two and were totally amorphous above generation four. The linear analogues were crystalline at all generations. This difference was also shown through the use of differential scanning calorimetry, yielding a glass transition temperature of 43°C for a fifth generation dendrimer and a melt transition of 153°C for the fifth generation linear analog. Using gel permeation chromatography it was shown that for generations one through four, the linear analogs had only a slightly larger hydrodynamic radius. At the higher generations, the difference between the hydrodynamic radii became much larger, with the linear analogs displaying hydrodynamic radii 40-50% larger then the dendrimers. This result was expected for the solvent being used, THF, because of the expectation that the linear analogs would adopt a random coil structure compared to the globular structure expected for the dendrimers.

A focus on the structure of dendrimers in solution allows for the prediction of certain solution properties. With each increase in dendrimer generation, the length of the dendrons will increase and therefore an increase of hydrodynamic radius would be expected. An increase in the radius of a dendrimer should result in decrease in the diffusion coefficient. This displays a simple prediction of properties, however other factors may also influence the hydrodynamic radius and the diffusion coefficient. Solvent interactions with the dendrimer have caused changes to the hydrodynamic radius and the diffusion coefficient[9, 16, 29, 34]. Dendrimers offer the ability to alter solvent access to the core, which may result in expansion or contraction of the interior microenvironment. If the microenvironment allows solvent access then the dendrons will extend and the dendrimer will swell, resulting in an increased hydrodynamic radius and a decreased diffusion coefficient. The opposite will be true as well; if solvent is excluded from the microenvironment then the dendrons will contract resulting in a more compact dendrimer with a smaller hydrodynamic radius and larger diffusion coefficient.

Literature studies have used pulsed field gradient spin-echo ^{1}H NMR and electrochemical techniques to show the changes in molecular radius and diffusion coefficient[9, 16, 18, 29]. Electrochemical techniques to calculate the diffusion coefficient include cyclic voltammetry, chronoamperometry, cyclic voltammetry, and voltammetry at a rotating disc electrode (RDE).

Abruña[29] and coworkers presented a comparison of PFGSE-NMR, cyclic voltammetry, and voltammetry at a rotating disc electrode. The dendrimers studied were polyamidoamine (PAMAM) functionalized with terminal terpyridyl and bipyridyl ruthenium complexes. The diffusion coefficient was shown to decrease with increasing

dendrimer generation for generations zero through four. This showed the hypothesized trend that increasing generation results in slower diffusion.

They determined that the difference between diffusion coefficient values from the different methodologies used was significant. The diffusion coefficients of a few of the dendrimers are shown below in **Table 1.1**. Cyclic voltammetry always yielded diffusion coefficients that were much smaller then RDE and PFGSE-NMR. The RDE values and PFGSE-NMR values were similar for lower generation dendrimers, but the difference between them increased at higher dendrimer generations.

Table 1.1: Diffusion coefficients of PAMAM dendrimers (cm^2/sec)

Dendrimer	**D_0 determined By CV**	**D_0 determined By RDE**	**D_0 determined By PFGSE-NMR**
G1	1.8×10^{-6}	3.7×10^{-6}	4.9×10^{-6}
G2	1.3×10^{-6}	2.9×10^{-6}	3.7×10^{-6}
G3	1.2×10^{-6}	3.2×10^{-6}	3.5×10^{-6}
G4	8.5×10^{-7}	2.1×10^{-6}	3.2×10^{-6}
G5	3.3×10^{-7}	8.1×10^{-7}	2.3×10^{-6}

Abruña investigated the differences between the techniques by focusing on the molecular diameter that can be found using the Stokes-Einstein equation:

$$D = \frac{kT}{6\pi R\eta} \tag{1.1}$$

where D is the measured diffusion coefficient, R is the radius of a spherical molecule, η is the viscosity of the solution, T is the temperature, and k is Boltzmann constant. The calculated diameters were then compared to the largest diameter of the molecule calculated by the use of average bond lengths. It was found that the diffusion coefficient from cyclic voltammetry yielded diameters that were much larger then the calculated

maximums. The diffusion coefficients from RDE yielded molecular diameters within range for lower generation dendrimers, but higher generation dendrimers resulted in impossible diameters. PFGSE-NMR diffusion coefficients always resulted in molecular diameters that were below the maximum calculated diameter. To test if the difference between the electrochemical methods and the NMR method was the presence of a counter-ion, PFGSE-NMR was repeated using a deuterated version of the electrochemical solutions. No change in diffusion coefficient was observed for the dendrimer, suggesting that the difference between diffusion coefficients stemmed from the electron transfer reaction. One concern was the fact that the redox unit was a terminal group and therefore the number of redox active groups increased from 4 to 8 to 16 to 32 to 64. The electrochemical techniques would be inaccurate if some of the redox centers did not undergo reduction/oxidation. Basic dendrimer structure dictates that at higher generations the terminal groups are arranged in a globular shape around the dendrimer core, which would result in the terminal redox groups being arranged in a circular architecture. The orientation of the dendrimer when near the electrode may place some of the redox active sites near the electrode, but some of the sites would be on the opposite side of the dendrimer and may not be able to communicate with the electrode.

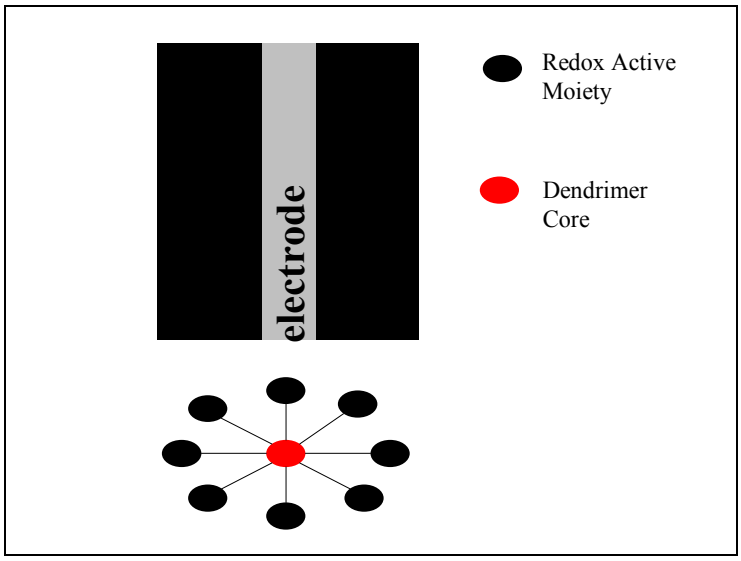


Figure 1.2: Cartoon depiction of a possible problem with Abruña's dendrimers and electrochemical determination of diffusion coefficients

Although the dendrimer could rotate, resulting in all of the redox active sites undergoing reduction or oxidation, the time necessary for the rotation would be slower than the time scales of the redox reaction and the electrochemical experiment. Since the RDE values become less accurate with increasing dendrimer generation it appeared that the increasing number of redox centers were the source of error. The data presented showed that all three techniques displayed a decrease in diffusion coefficient and increase in hydrodynamic radius with increasing dendrimer generation. However, the data was not the same for all three techniques and PFGSE-NMR was believed to give the most accurate diffusion coefficient values compared to the values calculated from the electrochemical techniques.

The diffusion coefficients of iron-sulfur core dendrimers were investigated by Gorman[9, 18] through the use of chronoamperometry and PFGSE-NMR. The different

techniques both showed a general trend of increasing molecular radius and decreasing diffusion coefficient as dendrimer generation increased. The experiments by Gorman showed some interesting information concerning the effects of dendron architecture and solvent dependence on the diffusion coefficient. For these studies iron-sulfur core dendrimers were synthesized with two different dendron architectures, one rigid and one flexible. The rigid dendron was based on a phenylacetylene repeat unit and the flexible dendron was based on a polybenzyl-ether repeat unit. The flexible dendrimers exhibited larger diffusion coefficients and smaller radii with chronoamerometry then with PFGSE-NMR. The rigid dendrimers exhibited the opposite, with PFGSE-NMR resulting in larger diffusion coefficients and smaller molecular radii. The difference between the values determined by each method was most likely due to the electrochemical differences between the two dendrimers. Direct comparison of diffusion coefficients in DMF and THF was not possible due to the different viscosities, but the hydrodynamic radius was comparable. The flexible dendrimers exhibited much larger hydrodynamic radii in THF, while the hydrodynamic radii of the rigid dendrimers remained nearly unchanged[18]. The difference in the hydrodynamic radius of the flexible dendrimer was likely due to the swelling of the dendrimer in THF and the contraction of the dendrimer in DMF. Little difference would be expected for the hydrodynamic radius of the rigid dendrimer because the dendrons were expected to maintain an extended structure independent of solvent.

A recent study by Gorman[16] focused on the difference between dendrimer constitutional isomer pairs. The dendrimers consisted of an iron-sulfur core and polybenzyl-ether dendrons. The dendrons were designed with one isomer extended, in a 3,5-disubstitution, and the other back-folded, in a 2,6-disubstitution. Using constitutional

isomers allowed for direct comparison of dendron architecture without having different molecular weight dendrons. It was hypothesized that the back-folded dendrimers would be more compact and would therefore exhibit a larger diffusion coefficient. PFGSE-NMR and chronoamperomentry were used to probe the diffusion coefficients of the different isomer pairs. **Table 1.2** shows the PFGSE-NMR data that supported the hypothesis that the back-folded isomers were more compact and had larger diffusion coefficients and smaller hydrodynamic radii. The calculated hydrodynamic radii showed a noticeable difference between the back-folded and extended isomers.

Table 1.2: Diffusion coefficients and hydrodynamic radii for constitutional isomers determined by PFGSE-NMR

Dendrimer	**Diffusion Coefficient ($x10^6$ cm^2/s)**	**R_H (Å)**
2,3	2.16	14.94
2B,3	2.57	12.55
3,2	2.43	13.28
3,2B	5.09	5.44
2,2	2.68	12.04
2B, 2B	5.98	5.40

Dendrimers have been shown to offer the ability to solublize cores that were previously insoluble in some solvents. The dendritic architecture has followed the hypothesized trends of increasing dendrimer generation causing larger hydrodynamic radii and small diffusion coefficients. These studies have also led to the investigation of how various techniques differ when determining the diffusion coefficient of a molecule.

The interesting solution properties of dendrimers led to further investigations into the electrochemical and photophysical properties of dendrimers.

Electrochemical Properties

The effect of encapsulation on redox active cores has also garnered attention for not only diffusion coefficient calculations, but also for the study of the kinetics and thermodynamics of redox active cores. The desire to use dendrimers for various applications requires a detailed knowledge of how dendrimer architecture affects redox properties. Areas of concern include: generational effects, dendron structure, and solvent interaction.

One of the major areas of electrochemical investigation is the kinetic electrochemical reversibility of dendrimers. The electrochemical reversibility of a molecule is governed by the ability of the redox active core to communicate effectively with the electrode. As dendrimer generation increases, the amount of mass surrounding the core increases resulting in an increased distance between the electrode and the core. As the distance between the core and the electrode increases the ability to communicate will decrease resulting in a decrease in kinetic reversibility.

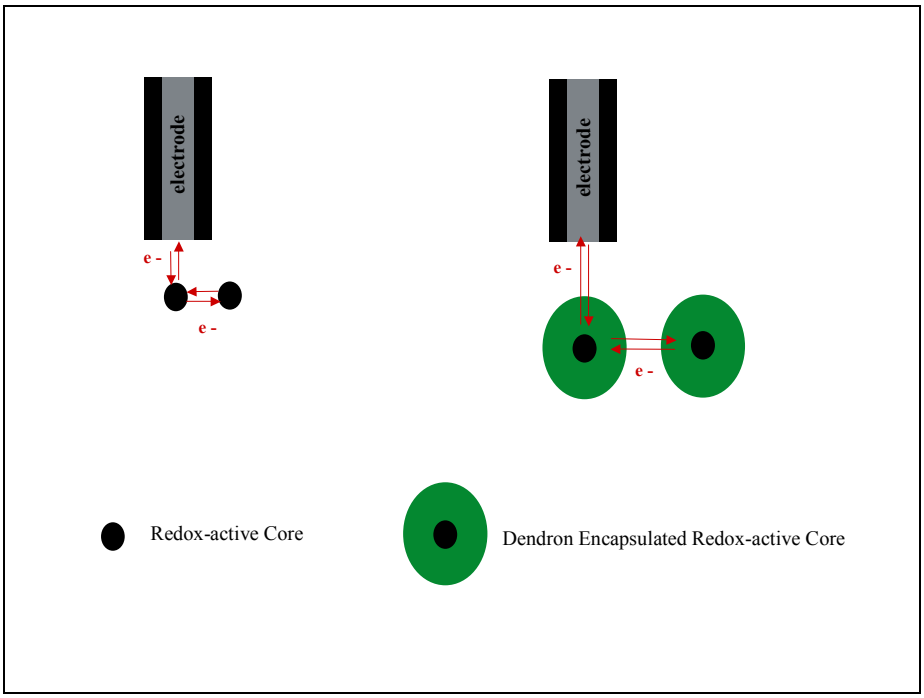


Figure 1.3: Cartoon depiction of encapsulation affecting the distance that an electron must travel

There have been many examples that have shown increasing dendrimer generation resulting in decreasing reversibility. All of these examples exhibited reversible or quasi-reversible electrochemistry at low generation dendrimers, but displayed irreversible electrochemical behavior at higher generations. Smith[35] reported decreasing reversibility with increasing generation for ferrocene core dendrimers and Gorman[9, 18] reported similar results with iron-sulfur core dendrimers. Kimura[36] also showed a change to irreversible electrochemical behavior with second-generation cobalt(II) porphyrin core dendrimers.

Although these studies all showed that electrochemical reversibility decreases with increasing dendrimer generation, they varied in the generation at which irreversibility was observed. One possible explanation for this difference was the wide

variety of dendrons used. In solution, dendrimers are constantly changing conformation suggesting that the core may not always be centrally located. If the core were able to move throughout the dendrimer then the distance between the electrode and the core could vary during measurements.

Gorman[9, 18, 19] considered the effect of dendron structure on the mobility of an iron-sulfur core. The studies included the use of two different dendron structures: flexible and rigid. The first generation of each dendron is shown in **Figure 1.4**. Computer simulations using quenched molecular dynamics showed that the rigid architecture resulted in the core of the dendrimer remaining more centrally located in the lowest energy conformations. Simulations on the flexible architecture suggested a more offset core location on average. Snapshots of two low energy conformations from the computer simulations are shown for fourth generation dendrimers in **Figure 1.5**.

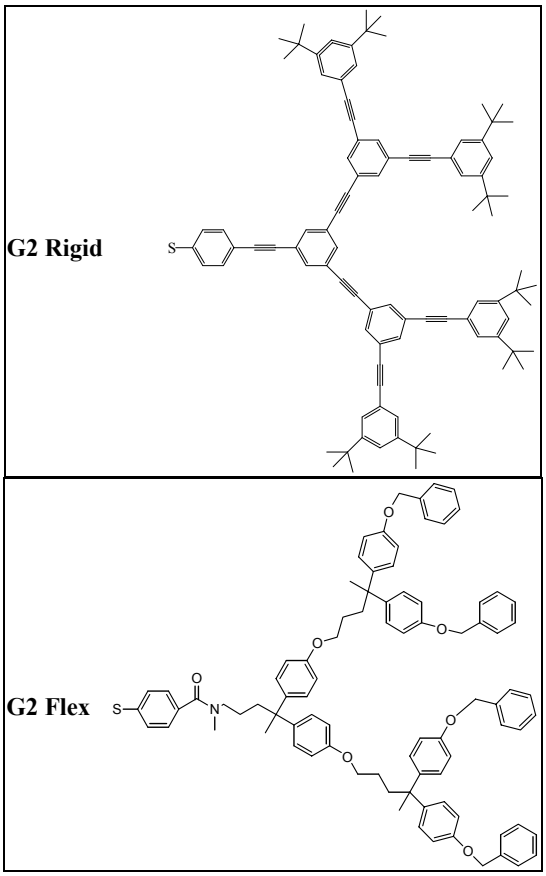


Figure 1.4: First generation rigid and flexible dendrons

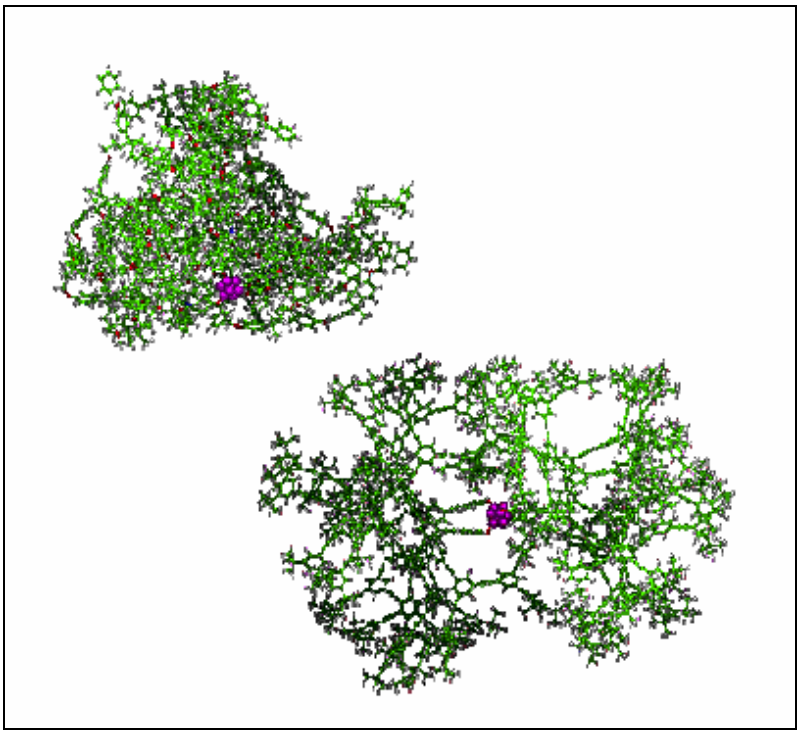


Figure 1.5: Snapshot of low-energy conformations determined by computer simulations showing the offset cores of fourth generation flexible (top) and rigid (bottom) dendrimers.

(The iron-sulfur core is shown in purple)

Absorption onto the electrode was a problem for electrochemical studies of higher generation rigid dendrimers, but rigid dendrimers up to third generation were studied. It was found that third generation rigid dendrimers displayed irreversible electrochemical behavior. However, third generation flexible dendrimers displayed quasi-reversible electrochemistry, but fourth generation flexible dendrimers showed irreversible electrochemistry. The data from these studies agreed with the hypothesis that dendron structure has a significant impact on the electrochemical properties of the redox active core. The studies also showed that the rigid dendrons would keep the core more centrally

located and therefore further from the electrode, causing a decrease in the kinetic reversibility.

The effect of dendrimer architecture and generation on the thermodynamic redox potential is not clearly understood. There are examples of dendrimer generation having no effect on redox potential, but there are also studies where there was a significant shift.

Gorman[9, 18] reported no change to the redox potential of iron-sulfur core dendrimers with increasing dendrimer generation. This observation was rationalized by using an energy level diagram showing the stabilization or destabilization that would be expected due to solvent interactions with the different redox states. The diagram, shown in **Figure 1.6**, shows that for redox couples that involve a neutral state and a charged state, solvent interaction with the charged state will change the energy gap between the two states and thus change the redox potential. However systems with two charged states would not show a difference in redox potential because both states will interact with the solvent and it should result in no change in the difference between states.

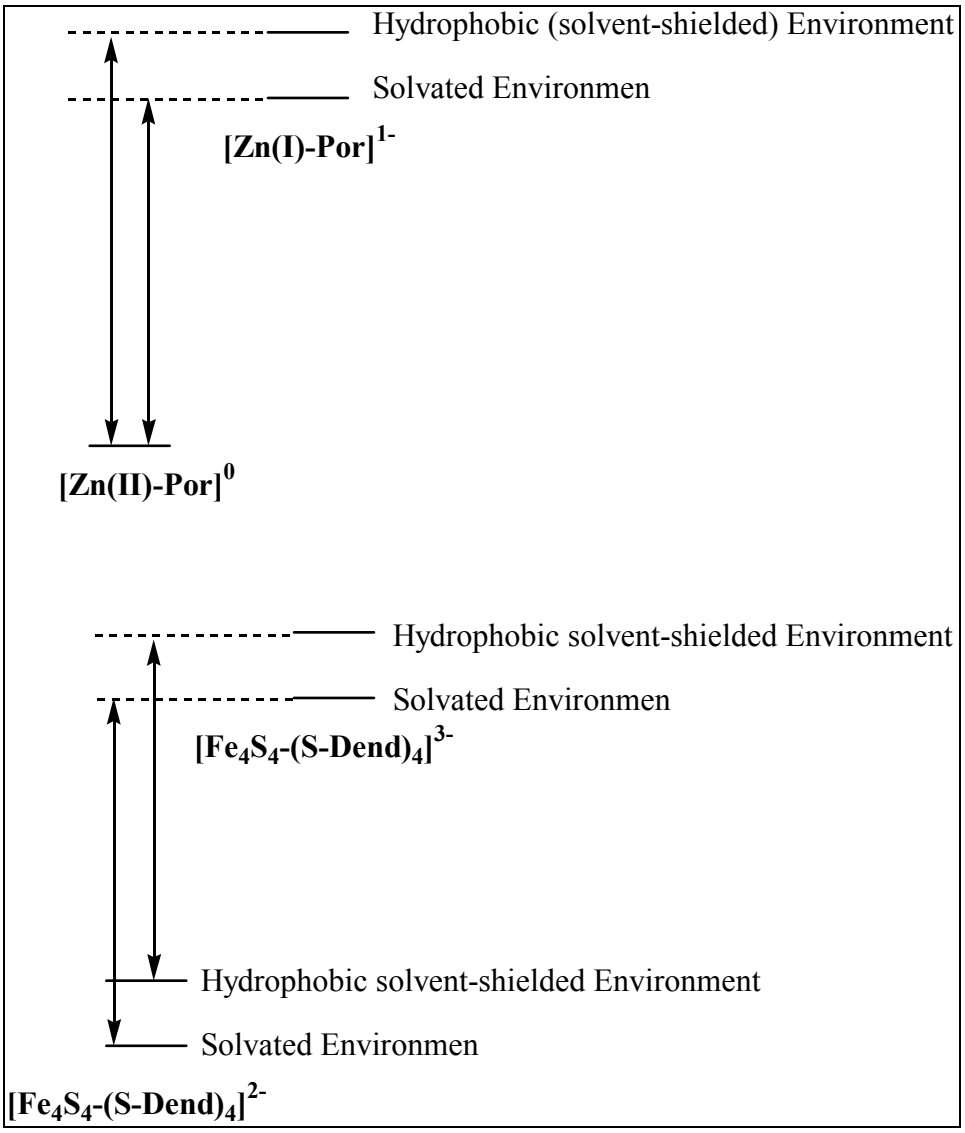


Figure 1.6: Energy level diagrams explaining the difference between dendrimers where a change in redox potential is observed and dendrimers that exhibit no change

However, some studies have shown shifts in the redox potential, but these shifts were very small and may fall within experimental error. Balzani[21] and Kaifer[20] reported the preparation and electrochemistry of identical symmetric, two-armed dendrimers based on a 4,4'-bipyridinium that exhibited a small change in redox potential with increasing dendrimer generation. The studies also showed that $E_{1/2}$ shifted to more

negative values as dendrimer generation increased for the same one-electron reduction. They concluded that the shift was due to the increasing hydrophobicity of the dendrons making solvation of the core more difficult. The inability to solvate the charged core will result in a desire for the molecule to adopt an uncharged state, thus making reduction favorable and shifting the redox potential to more negative values.

Two areas of concern exist with the experiments presented by Balzani and Kaifer. The first concern was the observation of precipitation of one of the species during electrochemical experiments. Precipitation in electrochemical experiments may cause fouling of the electrode and will change the concentration of the analyte in solution, making data inaccurate. The other concern was the size of the reported shifts in redox potential. The maximum shift in redox potential from G1 to G2 was reported as 5 mV. The maximum shift from G1 to G3 was reported as only 9 mV. These shifts in redox potential are very small and may have been within experimental error. The error for the electrochemical measurements was not included and therefore it was not possible to determine the size of the shift outside of experimental error.

Kaifer also reported the same trend of increasing dendrimer generation resulting in more negative redox potentials for unsymmetrical dendrimers with a 4,4'-bipyridinium core[7] and unsymmetrical dendrimers with a ferrocene core[8]. The unsymmetric dendrimers used were single-armed and may not have encapsulated the dendrimer core at generations zero through three. The unsymmetrical nature of the dendrimer would also make it possible for some dendrimers to be oriented with the unshielded core facing the electrode. This would result in the observed electrochemical values to be partially a function of

dendrimer orientation in solution. Thus this data did not clearly represent that the shift to more negative redox potentials was due to increasing dendrimer generation.

Diederich[13] showed shifts in the redox potential of iron porphyrin core dendrimers due to both generational and solvent effects. Generations zero through two of iron porphyrin core dendrimers with imidazole dendrons were investigated electrochemically. The data is shown in **Table 1.3**. In organic solvents, the Fe^{III}/Fe^{II} redox potential shifted to more positive values with increasing generation. The largest shift was between generations zero and one. In aqueous solution the largest shift was between generations one and two. The difference in the generational effects may be explained by the ability of water to be in close proximity to the core and therefore stabilize the charge on the iron in the zero and first generation dendrimers. The second-generation dendrimer may provide more of a barrier to the water molecules therefore not allowing stabilization of the core. This explanation would explain both the large change in redox potential and the shift towards more positive potential.

Table 1.3: Redox potentials of iron porphyrin core dendrimers in various solvents (V vs. SCE)

Dendrimer	**CH_2Cl_2**	**MeCN**	**H_2O**
G0	-0.21	-0.24	-0.29
G1	+0.08	-0.01	-0.25
G2	+0.10	+0.09	+0.09

Smith[35] showed similar trends in redox potential using ferrocene cores surrounded by symmetric Newkome-type dendrons. Generations zero through three were investigated in various organic solvents. The redox potentials in methylene chloride and

acetonitrile are shown in **Table 1.4**. The data showed a shift towards more positive potentials with increasing generation. The error was reported as ±5mV, so the shifts were not due to experimental error. The difference between G0 and unmodified ferrocene was approximately 300mV in both solvents. The difference between redox potentials remained the same for G0 to G1 and G1 to G2 in methylene chloride, but in acetonitrile the difference between G1 and G2 was larger then the difference between G0 and G1. This suggested encapsulation beginning at G0, but complete encapsulation may not have been achieved at generation two in acetonitrile.

Table 1.4: redox potentials of ferrocene core dendrimers
(V vs. Ag/Ag^{+})

Dendrimer	**CH_2Cl_2**	**MeCN**
Unmodified Ferrocene	0.583	0.490
G0	0.875	0.786
G1	0.914	0.818
G2	0.953	0.929

Gorman's[16] studies of constitutional isomers investigated the difference of redox potential based on dendron structure. It was hypothesized that the back-folded dendrimers would encapsulate the iron-sulfur core to a greater degree, making the core harder to reduce. Making the core harder to reduce would cause a shift towards more negative redox potentials. The expected trend was observed, as shown in **Table 1.5**.

Table 1.5: Redox potentials of iron-sulfur core constitutional isomer dendrimers (V vs. Ag/Ag^{+})

Dendrimer	$E_{1/2}$
2,3	-1.514
2B,3	-1.519
3,2	-1.494
3,2B	-1.623
2,2	-1.519
2B, 2B	-1.614

Studies of the electron transfer kinetics of dendrimers have shown effects similar to those described for the thermodynamic properties. The globular shape of dendrimers leads to an increased distance from the electroactive core to the periphery of the dendrimer as the generation increases. This increased distance is the distance that an electron must travel to get from the core to an electrode or from the electrode to the core. An increase in the distance to be traveled would result in longer times necessary to travel and therefore slower kinetics would be expected.

Gorman's[9, 18] studies of rigid and flexible dendrimers showed how electron transfer rates vary based on dendron architecture. Increasing dendrimer generation resulted in decreasing electron transfer rates for both architectures. A comparison of the two architectures, at similar molecular weights, showed that the flexible dendrons displayed faster electron transfer kinetics then the rigid dendrons. Generational and architectural comparisons are shown in **Figure 1.7**.

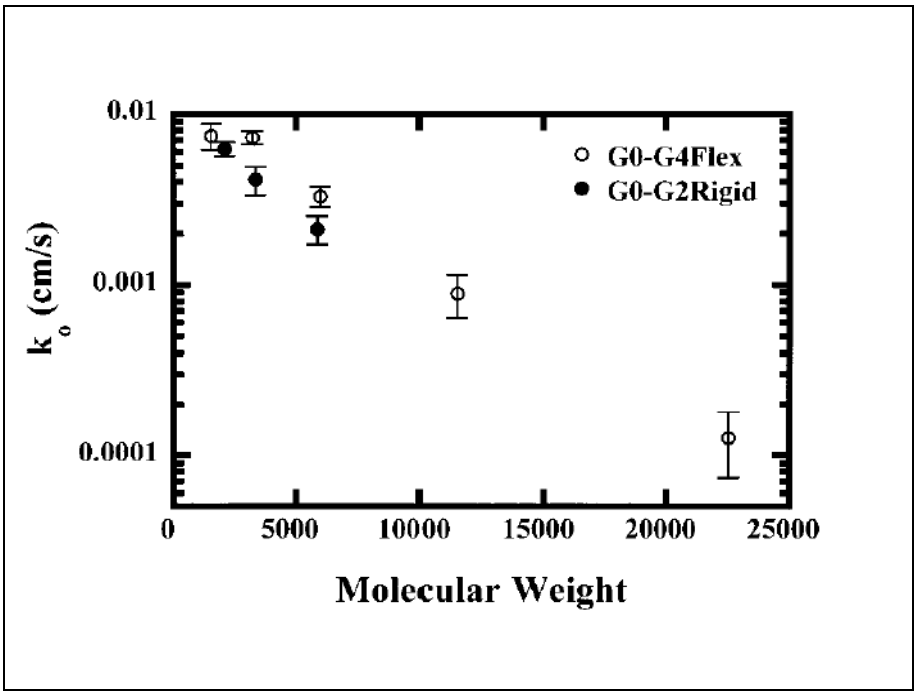


Figure 1.7: Heterogeneous electron rate transfer constants for flexible and rigid iron-sulfur core dendrimers

Further investigation of the rigid and flexible dendrimer architectures by Gorman[9, 18] was necessary because of the presence of conjugation within the rigid structure. To isolate any differences due to the presence of conjugation the electron transfer rate was compared for dendrimers of similar radii of gyration. The heterogeneous electron transfer rate as a function of radius is shown in **Figure 1.8**. The generational trend of decreasing rates for increasing generation was the same as observed for the molecular weight studies. The rigid dendrimers showed a small change in electron transfer rate with increasing generation, but the difference between electron transfer rates increased with increasing generation for the flexible dendrimers. This data showed that the rigid architecture transferred electrons more efficiently per unit length then the flexible dendrons.

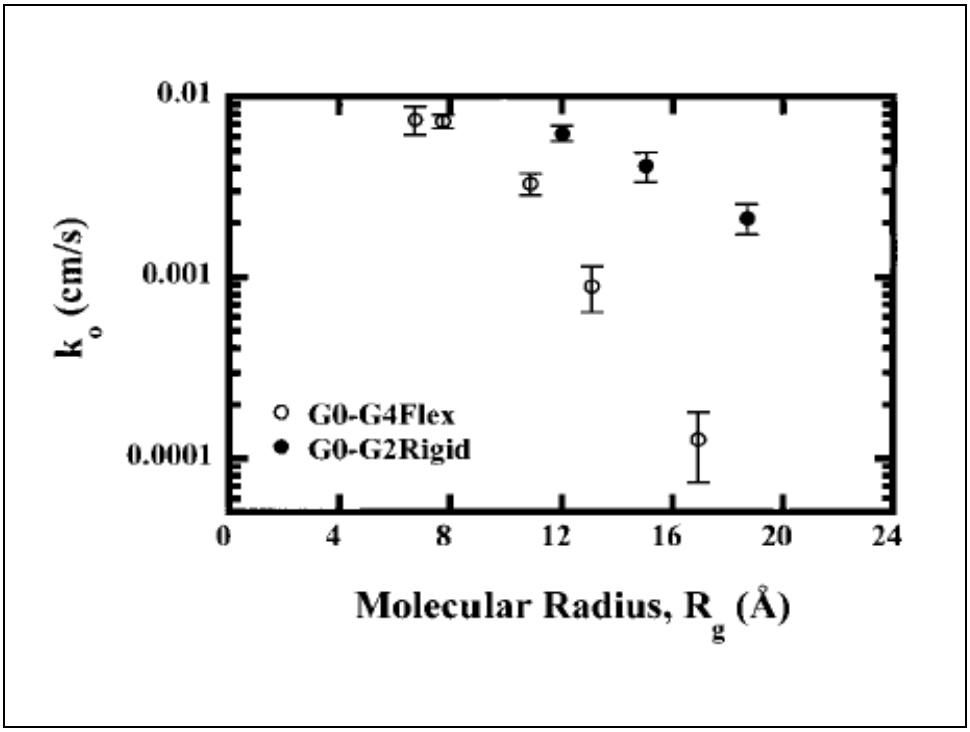


Figure 1.8: Heterogeneous electron transfer rates as a function of molecular radius for flexible and rigid iron-sulfur core dendrimers

The constitutional isomer pairs studied by Gorman[16] also offered information concerning the effect of dendron architecture on the rate of electron transfer. A cartoon schematic of this phenomenon is shown in **Figure 1.9**. Computer simulations suggested that the back-folded dendrons kept the core more centrally located, resulting in a larger distance between the redox active core and the electrode. Electrochemical characterization showed that the extended architecture exhibited rates of electron transfer from 2.5x to almost 6x faster then the back-folded architecture.

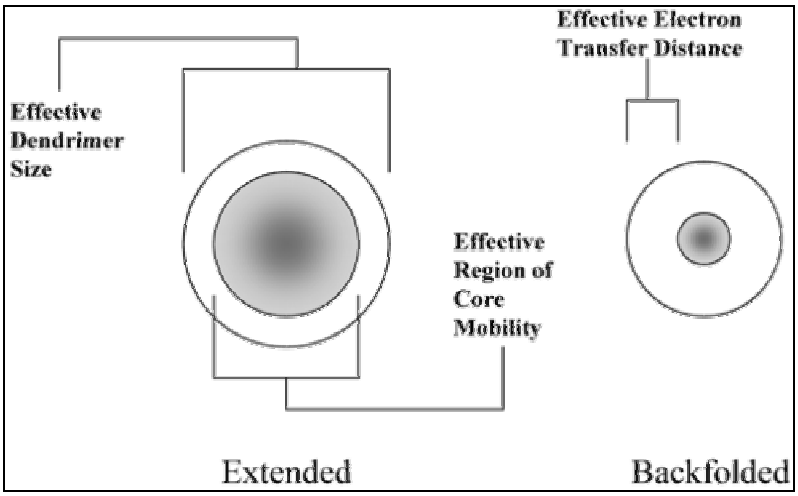


Figure 1.9: Cartoon depiction of effective electron transfer distance differences between extended and backfolded iron-sulfur core dendrimers

Photophysical properties

Investigations of dendrimers with luminescent cores have also drawn much interest. It was hypothesized that encapsulation could reduce the number of quenching pathways by forming a physical barrier around the core. This barrier would prevent quenching from small molecules like solvent molecules and oxygen by not allowing access to the core. Encapsulation should also prevent self-quenching since the excited cores would be kept apart by the dendrons surrounding each core. A decrease in the number of available nonradiative quenching pathways should result in an increase in the observed quantum yield and fluorescent lifetime.

Turro[37] is often credited with the first photophysical investigations using dendrimers. Turro used ruthenium-tris-2,2'-bipyridine core dendrimers and studied quenching due to the presence of methyl viologen. Ruthenium-tris-2,2'-bipyridine fluorescence was quenched through electron transfer to methyl viologen when the two

species were in close proximity. Turro's studies showed that unmodified ruthenium-tris-2,2'-bipyridine and first generation dendrimers were not quenched by the presence of methyl viologen. These observations led to the hypothesis that the methyl viologen was not able to get close enough to the ruthenium- tris-2,2'-bipyridine due to charge repulsion. At higher generations the charge of the core was buried within the dendrimer and not strong enough to repel the methyl viologen, allowing the core and the methyl viologen to be close enough to allow for electron transfer and hence quench the fluorescence.

Fréchet[11, 38] used self-assembled lanthanide core dendrimers to study the variations of quantum yield with increasing dendrimer generation. The dendrimers were excited at 289nm, corresponding to the absorption of the lanthanide ion core. These studies showed a significant increase in quantum yield with increasing dendrimer generation. Balzani[4, 22] observed the same trends with ruthenium core dendrimers and ruthenium tris-2,2'-bipyridine core dendrimers. In both studies, the dendrons consisted of polybenzyl-ether groups with phenyl terminal groups and napthyl focal groups. The comparison of the unmodified core and the different dendrimer generations are shown in **Table 1.6**. The numbers in parentheses corresponds to the dendrimer generation. The quantum yields values followed the expected trend of increasing dendrimer generation resulting in increased quantum yield.

Table 1.6: Quantum yield and emission lifetimes of ruthenium core dendrimers

Molecule	λ_{max} (nm)	Φ_{em}	τ (μs) deaerated	τ (μs)
$[Ru(bpy)_3]^{2-}$	611	0.016	0.990	0.172
$[Ru(G1)_3]^{2-}$	614	0.019	1.16	0.191
$[Ru(G2)_3]^{2-}$	611	0.029	0.990	0.316
$[Ru(G3)_3]^{2-}$	609	0.048	1.04	0.562

The lifetime comparison of aerated solutions versus deaerated solutions demonstrated the ability of dendrimers to protect against quenching due to oxygen. The lifetimes in aerated solution showed an increase with increasing dendrimer generation. The difference between the lifetimes in aerated solution and deaerated solution also decreased with increasing dendrimer generation. The smaller difference between lifetimes suggested that the dendrons were protecting the core from oxygen in the aerated solution and preventing quenching.

Aida[24] used a poly(phenyleneethynylene) core dendrimer to study both generation effects and concentration effects. The rigid, conjugated backbone was surrounded by polybenzyl-ether dendrons, which were designed for better solubility and the ability to provide energy transfer functionality. Aida reported quantum yields of near 1 for third and fourth generation dendrimers in dilute solution. Second generation dendrimers exhibited a quantum yield of 0.58. It was concluded that increasing dendrimer generation was responsible for the increase in quantum yield.

Aida also investigated the ability of dendrimer to prevent self-quenching. Fourth generation dendrimers still showed a quantum yield of one when the absorbance was equal to 0.1, which was considered concentrated enough to observe self-quenching.

Generations two and three showed decreases in quantum yield with increasing concentration. This data showed that self-quenching decreased as dendrimer increased.

Kaifer[39] used asymmetrical Newkome-type dendrons surrounding dansyl cores and showed that the quantum yield increased with increasing dendrimer generation. The lifetimes of these dendrimers also increased with increasing generation. Protection of the core from small molecules quenching was shown through the use of a β-cyclodextrin binding experiment. The basic dansyl group exhibited an increase in fluorescence intensity when exposed to β-cyclodextrin. The increase in fluorescence intensity was not as extreme for the first generation dendrimer. Second and third generation dendrimers showed almost no change at all, suggesting that little or no β-cyclodextrin binding was occurring.

Castellano[40] attempted to use a different approach to show encapsulation effects. This approach compared the quantum yields of single armed dendrimer and a three-armed dendrimer. The dendrimers were based on ruthenium- tris-2,2'-bipyridine cores with the arms consisting of coumarin terminal groups. Comparison of the quantum yields of the one-armed dendrimer and the three-armed dendrimer showed only a slight difference. However, both of the dendrimers showed an increase in quantum yield compared to unmodified ruthenium- tris-2,2'-bipyridine. The lifetimes exhibited the same trend as the quantum yields, with the dendrimers showing longer lifetimes then the unmodified core, but little change was observed between the dendrimers.

All of the studies concerning the photophysical properties of dendrimers have exhibited increasing quantum yield and lifetimes with increasing dendrimer generation. The increase in quantum yield has been hypothesized to be linked to decreasing the

availability of nonradiative quenching pathways such as small molecule quenching and self-quenching.

Energy Transfer

Interest in dendrimers for optical applications led to investigation into the possibility of energy transfer within the dendritic architecture. The ability to transfer energy requires a donor and an acceptor. In a dendritic molecule, the donor would be the dendron terminal group and the acceptor would be the emitting core. This design benefits from the geometrical increase in the number of terminal groups with increasing dendrimer generation. Shown in **Figure 1.10** is an energy level diagram depicting the transfer of an exciton from donor to acceptor.

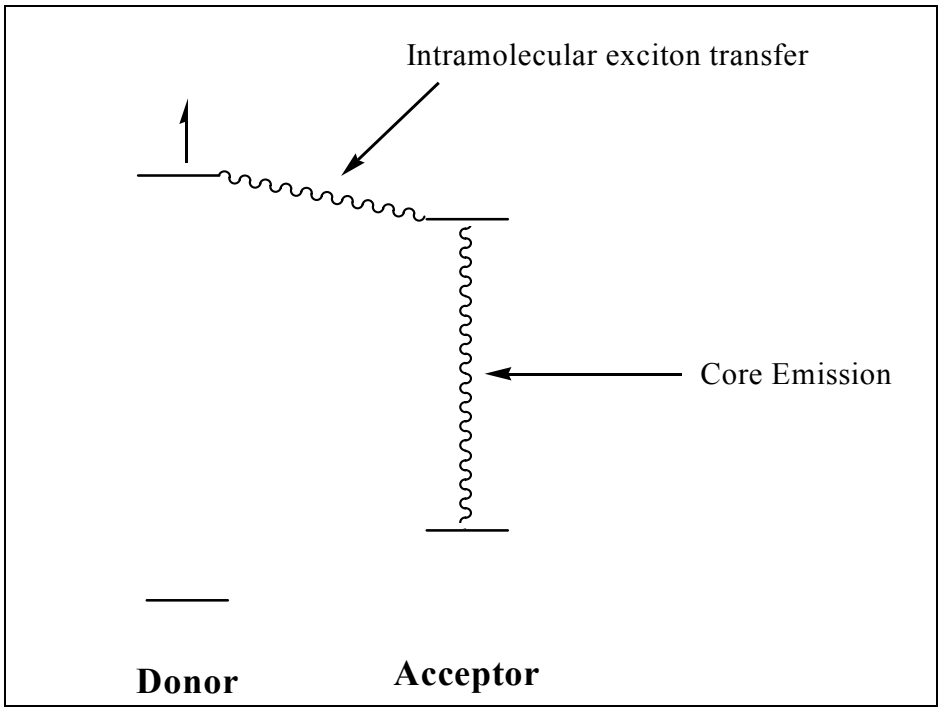


Figure 1.10: Energy level diagram depicting intramolecular exciton transfer

Prediction of efficient energy transfer is based on the overlap of the emission spectrum of the donor and the absorbance spectrum of the acceptor. A large overlap should result in more efficient energy transfer. Dendrimers designed for optical applications can thus be designed to maximize energy transfer capabilities.

It has been hypothesized that the mode of energy transfer within dendrimers is the Förster mechanism[11, 23, 33, 41]. The mode of energy transfer in the Förster mechanism is through space, compared to the through bond mechanism of Dexter. The Förster mechanism has a maximum radius of energy transfer known as the Förster radius. It is this restriction that may cause energy transfer efficiency in dendrimers to decrease with increasing dendrimer generation because as dendrimer generation increases the distance between the core and the terminal groups should increase.

Hawker[33] compared the energy transfer abilities of dendrimers and their linear analogs. The study used polybenzyl-ether dendrons, which have been previously shown to facilitate energy transfer[11, 38]. The linear molecules exhibited large decreases in energy transfer efficiency with increasing generation. However, the dendrimer equivalents exhibited only a small decrease in efficiency with increasing generation. This conclusion was consistent with the concept that dendrimers adopted a globular shape at higher generations. The globular form would keep the absorbing units close to the core allowing for Förster energy transfer. The linear molecules were expected to spread out in solution making energy transfer from the furthest absorbing units nearly impossible.

Moore[41, 42] used a group of one-armed perylene core dendrimers to investigate directed energy transfer in dendrimers. The dendrons were designed with conjugation in order to facilitate energy transfer and to create a system that favored energy transfer in

the direction of the core. UV-Vis absorption was used to show that the number of absorbing terminal groups increased with increasing dendrimer generation. Steady-state fluorescence with excitation at 310nm was then used to determine energy transfer efficiencies of the different generations. The 310nm wavelength was chosen because it was near the dendron absorption and therefore any emission from the perylene core would be due to energy transfer. Emission from the perylene core was observed thus indicating intramolecular energy transfer. The resulting energy transfer quantum yields are shown in **Table 1.7**.

Table 1.7: Energy transfer quantum yield values for perylene-terminated dendrimers (Excitation wavelength=310nm)

Dendrimer	**λ_{max} (nm)**	**Φ_{ET}**
G1	482, 515	0.95
G2	483, 516	0.91
G3	483, 517	0.95
G4	483, 517	0.91
G5	486, 519	0.85
G6	487, 519	0.54

The data from this study showed a decrease in the energy transfer quantum yield with increasing dendrimer generation. The result corresponds with the hypothesis that the mode of energy transfer is the Förster mechanism, where an increase in donor-acceptor distance would result in decreased energy transfer efficiency.

The photophysical studies of dendrimers have shown that dendritic architecture allows for enhancement of the quantum yield and lifetimes of various luminescent cores.

Dendrimers were able to prevent quenching and were shown to allow energy transfer from the dendrons to the core. These trends suggest that dendrimers can be specifically designed for different optical applications.

Dendrimers offer a unique architecture that has been shown to provide chemists with the ability to alter various core properties through dendron design. Dendrimers provide access to the electrochemical and photophysical properties of the dendrimer core, while also allowing for modification of these properties.

Rhenium-Selenide Core

Experimental work on rhenium-selenide cores began as part of Chevrel phase research. Rhenium-selenide core molecules are part of a larger group of molecules known as hexanuclear rhenium chalcogenides. The first example of a molecule with a rhenium chalcohalide core was in 1971, $Re_6Q_4X_{10}$ (Q=Se, Te; X=Cl, Br), by Fedorov[43]. Leduc, Perrin, and Sergent[44] also showed examples of octahedral rhenium-selenide cores in 1983. Since that time there has been much work done on these cores including reactivity, photophysical, and solubility experiments.

Rhenium chalcohalides exist in many different states. In the molecular form, they may posses a neutral charge, 1-, 2-, 3-, 4-, or 2+. The polymeric forms of these clusters have also drawn much interest. Rhenium chalcohalides have been shown to adopt zero-, one-, two-, and three-dimensional structures depending on the molecular formula. The structures of the multidimensional forms vary depending on the geometry and connectivity of the ligands and the intercluster bridging.

X-ray structure elucidation has offered much information about the structure of rhenium-selenide core molecules. X-ray studies of rhenium-selenide cores have shown

that the rhenium atoms exist in an octahedral arrangement with the selenium atoms capping the faces of the octahedron. A depiction of the rhenium-selenide core as described is shown in **Figure 1.11**. The selenium atoms are each attached to three different rhenium atoms and are therefore denoted as having μ_3 connectivity. Other ligands attach to the apices of the octahedral rhenium atoms.

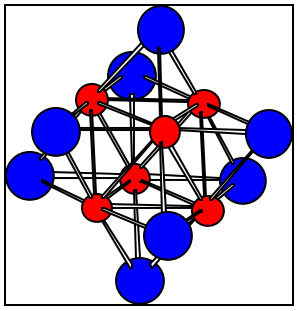


Figure 1.11: Octahedral rhenium-selenide cluster
(rhenium atoms are depicted in red and selenium atoms in blue)

Many different rhenium-selenide core molecules have displayed similar dimensions despite changes to the apical ligands. **Table 1.8** shows a list of mean Re-Re and Re-Se bond lengths from the Holm[45, 46] papers. The fact that the dimensions of the core remain unchanged show that the core is robust and its properties should not change significantly with changes to the ligands.

Table 1.8: Mean bond lengths (Å) and bond angles (degrees) of rhenium-selenide clusters

	$Cs_4Re_6Se_8I_6$	$(Bu_4N)_3[Re_6Se_8I_6]$
Re-Re mean distance	2.625	2.624
Re-Se mean distance	2.519	2.506
Re-I mean distance	2.793	2.773
Re-Re-Re mean angle (Triangular faces)	60.0	60.0
Re-Re-Re mean angle (equatorial faces)	90.0	90.0
Re-Re-Se mean angle	58.6	58.4
Re-Se-Re mean angle	62.8	63.1
Se-Re-Se mean angle	89.9	89.9

Holm used the term "dimensional reduction" to describe the process of going from a three dimensional form to a zero dimension form by the addition of a halide salt[45]. This process is shown in **Figure 1.12**, although this was not necessarily the mechanism. The main goal of dimensional reduction was to produce a soluble, zero-dimensional form of rhenium chalcogen clusters.

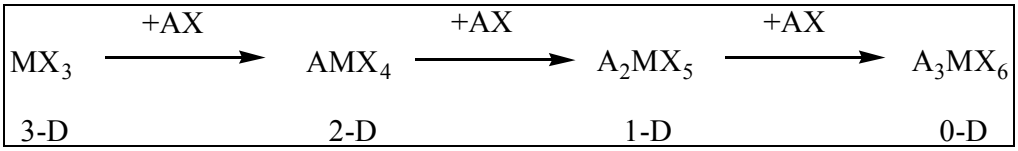


Figure 1.12: Dimensional reduction

Holm has done extensive work in the pursuit of a soluble rhenium chalcohalide cluster[45, 47-50]. The work began with solid-state synthesis followed by solution chemistry designed to maintain the rhenium chalcohalide core.

The first example of dimensional reduction of a rhenium-selenide core was completed using the 2-dimensional $Re_6Se_8Cl_2$, which was converted to the 0-dimension $Tl_5Re_6Se_8Cl_7$ after the addition of 5 equivalents of TlCl. While this dimensional reduction produced the desired product, the product was found to be insoluble. Since the desired result of this experimentation was the production of a soluble form of $[Re_6Se_8]^{2+}$, this example was considered unsuccessful. However, the formation of $Tl_5Re_6Se_8Cl_7$ did show that a potential pathway existed to form a zero-dimension molecule. In order to investigate other clusters, Holm decided to switch to another halide salt and chose cesium halides[45]. Dimensional reductions using CsCl and CsBr resulted in one-dimensional forms being isolated. The other halide, CsI, resulted in a soluble, zero-dimension $[Re_6Se_8]^{2+}$ cluster: $Cs_4Re_6Se_8I_6$.

This solid, $Cs_4Re_6Se_8I_6$, did not follow the same pattern as the rest of the investigated molecules when taken onto the next reaction. All of the solids were stirred in acid and then base was added, with no change being observed. $Cs_4Re_6Se_8I_6$ was dissolved in hydriodic acid, but adding base to the solution resulted in a color change from red to yellow. At the time of publication, investigation of this phenomenon had just begun and it was hypothesized that OH^- was exchanging for I^- to form $[Re_6Se_8(OH)_6]^{4-}$. This was the only molecule to exhibit such behavior. It was hypothesized that the stirring in aqueous acid protonated one of the chalcogen atoms and thus it was believed that the species isolated following acid work-up was $[Re_6Se_7(SeH)I_6]^{3-}$. In most of the molecules

studied, it was possible to isolate both a protonated and an unprotonated form of the product based on the equilibrium below:

$$[Re_6Q_8X_6]^{4-} + H^+ \rightleftharpoons [Re_6Q_7(QH)X_6]^{3-} \quad (1.2)$$

The difference between the protonated and unprotonated species was observed using UV-Vis spectroscopy. In most of the species, except $[Re_6S_7(SH)I_6]^{3-}$ and $[Re_6Se_7(SeH)I_6]^{3-}$, the presence of a proton was characterized by new peaks between 500nm-600nm in the spectra of the protonated species. The $[Re_6S_7(SH)I_6]^{3-}$ showed absorbance at higher wavelengths then the unprotonated species, but did not display any new peaks. The other exception, $[Re_6Se_7(SeH)I_6]^{3-}$, displayed a peak around 600nm, but there was no other species isolated and therefore no other spectrum available for comparison.

The inability to isolate the unprotonated $[Re_6Se_8I_6]^{4-}$ species led to further investigation of this cluster. The possibility of protonation was developed following x-ray diffraction and elemental analysis showed three cations (tetrabutylammonium, +1 charge) were associated with each cluster. Since the core should be 4-, but the cations present provided only a 3+ charge, it was hypothesized that a proton was present. The presence of the proton could not be determined using x-ray diffraction or elemental analysis. There was no mention of ^{1}H NMR or ^{77}Se NMR attempts to confirm the presence of a proton. Attempts at electrochemical characterization of a similar compound, $[Re_6S_8Br_6]^{3-}$ showed that reduction was the initial redox reaction, therefore showing that the initial charge was 3- and no proton was present. Further experimentation using EPR offered further proof that the actual species recovered were

$[Re_6S_8Br]^{3-}$ and $[Re_6Se_8I_6]^{3-}$, with no proton present. Following this experimentation, it was hypothesized that these two clusters were isoelectronic with $[Mo_6Cl_{14}]^-$ and $[W_6Br_{14}]^-$, $23e^-$ clusters with S=1/2[51].

An examination of the energy levels of the rhenium-selenide core has not been shown in the literature, but there have been similar systems whose energy levels have been explored. Hughbanks and Hoffman[52] have studied Mo_6X_8 systems, where X= S, Se, or Te. Although the cores are considered isoelectronic, the charge on the two cores were different. Hughbanks and Hoffman specifically examined the Mo_6S_8 core, which has a 4- charge compared to the 2+ charge on the Re_6Se_8 core. Hughbanks and Hoffman showed two different energy level diagrams, one for just the $[Mo_6S_8]^{4-}$ core and one that included the perturbation that occurred when each Mo atom is capped with a sulfur atom, resulting in $[Mo_6S_{14}]^{16-}$. These diagrams are shown below in **Figure 1.13**.

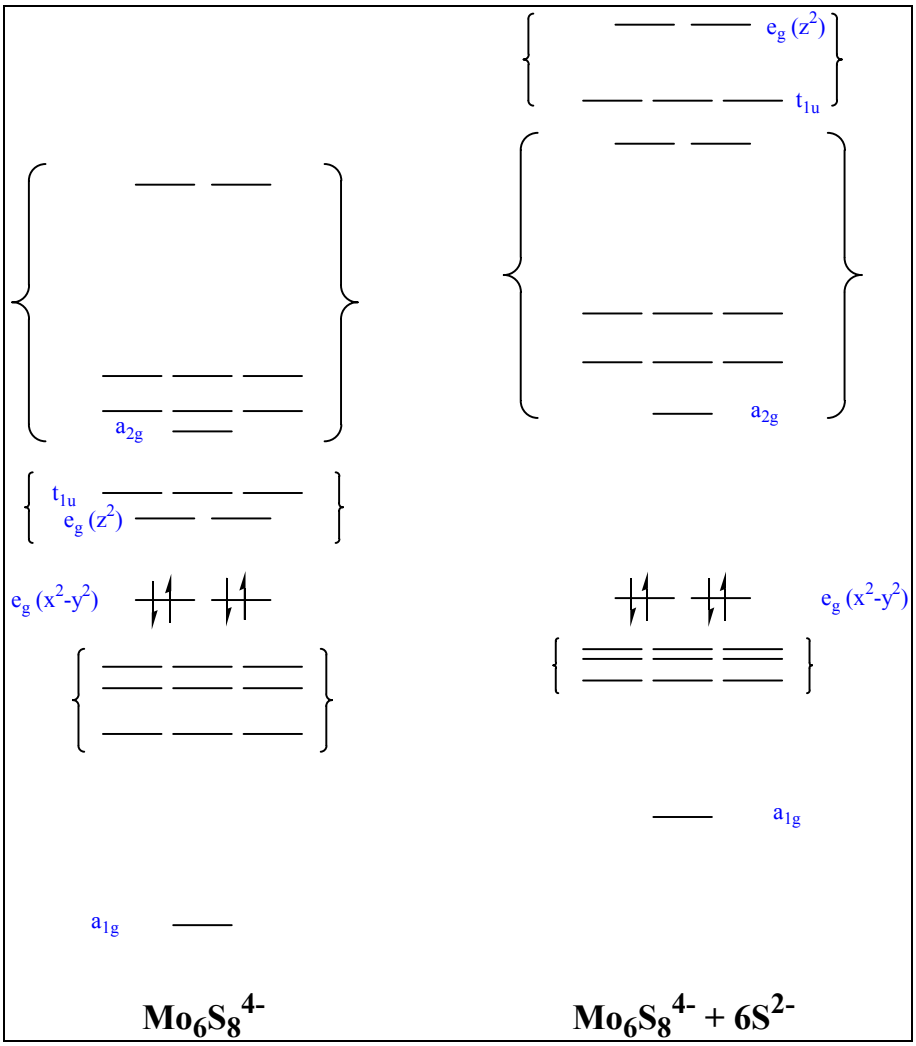


Figure 1.13: Energy level diagrams for $[Mo_6S_8]^{4-}$ cores

The energy level diagrams show that the HOMO-LUMO gap changes when adding the apical sulfurs. The HOMO remains the same, but the unoccupied orbitals move to a higher energy.

Gray[53, 54] was the first to investigate the photophysical properties of multiple rhenium chalcogen molecules. A partial list of these molecules and their corresponding photophysical properties are shown in **Table 1.9**. The absorption spectra of these

molecules showed a ligand to metal charge transfer (LMCT) band that occurred between 210nm-500nm. Excitation at the ligand to metal charge transfer band resulted in emission between 600nm-1000nm. The $[Re_6Se_8(solvent)_6]^{2+}$ molecules exhibited the highest emission energies, largest quantum yields, and the longest lifetimes when measured in excess ligand. Interestingly, when the emission of $[Re_6Se_8(pyridine)_6]^{2+}$, $[Re_6Se_8(DMF)_6]^{2+}$, $[Re_6Se_8(Me_2SO)_6]^{2+}$ clusters were measured in acetonitrile, the resulting spectra matched exactly with the $[Re_6Se_8(MeCN)_6]^{2+}$ spectrum. This suggested that the other solvent ligands were replaced by acetonitrile, although there was no experimental data showing if one of the other solvents acted similarly when in excess. The $[Re_6S_8X_6]^{4-}$ (where X= Cl, Br, I) clusters exhibited increasing quantum yields, lifetimes, and emission energies with increasing charge density.

Table 1.9: Selected photophysical properties of rhenium-chalcogen molecules (Φ_{em} is the quantum yield, τ_0 is the lifetime, k_r is the rate of radiative decay, and k_{nr} is the rate of nonradiative decay; All solutions had absorbance >0.1 at excitation wavelength)

Cluster	Φ_{em}	τ_0 (μs)	k_r ($s^{-1}10^4$)	k_{nr} ($s^{-1}10^5$)
$[Re_6S_8Cl_6](Bu_4N)_4$	0.031	5.1	0.61	1.90
$[Re_6S_8Br_6](Bu_4N)_4$	0.012	3.9	0.31	2.53
$[Re_6S_8I_6](Bu_4N)_4$	0.011	2.6	0.42	3.80
$[Re_6Se_8(PEt_3)_6]I_2$	0.068	10.8	0.63	0.86
$[Re_6Se_8(MeCN)_6](SbF_6)_2$	0.100	14.8	0.68	0.61
$[Re_6Se_8(pyridine)_6](SbF_6)_2$	0.163	14.0	1.23	0.63
$[Re_6Se_8(DMF)_6](SbF_6)_2$	0.203	18.9	1.07	0.42
$[Re_6Se_8(Me_2SO)_6](SbF_6)_2$	0.238	22.4	1.06	0.34

Studies using PEt_3 as a ligand also yielded important data. PEt_3 is a neutral ligand and therefore the overall charge on the core will be 2^+ and the photophysical data would be expected to be similar to that of the $[Re_6Se_8(solv)_6]^{2+}$ clusters. The $[Re_6Se_8(PEt_3)_6]^{2+}$ molecule showed decreased emission energy, quantum yield, and lifetime when compared to the solvent clusters. The strength of the rhenium-phosphorous interaction was considered to be very strong, especially when compared to the solvent ligands[47, 48].

It can be hypothesized that there is a trade-off between interaction strength and photophysical properties of the core, with a stronger interaction resulting in decreased quantum yield and shorter lifetime. This tradeoff was also observed with the $[Re_6Se_8(solv)_6]^{2+}$ clusters. Since acetonitrile was able to replace the other solvents it would appear that acetonitrile had the strongest interaction and the acetonitrile cluster displayed the lowest quantum yield and lifetime of the solvent clusters. Direct comparison of the solvent clusters and the PEt_3 cluster was not possible because of the use of a different counter-ion (I_2 vs. $(SbF_6)_2$), which may have influenced the photophysical properties. These studies did showcase the photophysical properties of the rhenium-selenide cluster, while also suggesting that the design of the attached ligands may influence the quantum yield and lifetime.

The rates of nonradiative decay, shown in **Table 1.9**, for the rhenium-chalcogen molecules were larger then those reported for the isoelectronic molybdenum and tungsten clusters. As expected the rate of nonradiative decay increased as the fluorescent lifetime decreased. The rates of radiative decay were similar for rhenium, molybdenum, and tungsten clusters.

Batail[51] detailed the electrochemical properties of rhenium, molybdenum, and tungsten chalcogen halides. The $E_{1/2}$ values for rhenium cores ranged from +1.36V to –0.22V. The only 3+/2+ rhenium cluster had an $E_{1/2}$ value of 1.01V in methylene chloride. Electrochemistry of rhenium chalcogen cores were shown to be accessible through studies including $(Bu_4N)_4[Re_6S_8X_6]$ (X=Cl, Br) that displayed $E_{1/2}$ values of 0.3V and 0.29V respectively. Only two studies revealed negative $E_{1/2}$ values, they consisted of the $[Re_6Q_5Cl_9]^{1-/2-}$ (Q = S, Se) couples.

Rhenium-selenide core dendrimers

Rhenium-selenide core dendrimers have been previously synthesized and characterized by Zheng[6, 55]. The first pair of dendrimers prepared by Zheng used pyridyl linkages to attach two different types of dendrons[55]. The dendrons are shown in **Figure 1.14**. Preparation of these compounds was completed using a convergent synthesis scheme. Completion of ligand exchange was assumed when the solution became transparent, following approximately 12 hours of refluxing in chlorobenzene. Dendrimer formation was characterized by shifts observed in the ^1H NMR, with all proton peaks shifted downfield following ligand exchange. The largest shifts were observed for the pyridyl protons closest to the core, with shifts of 0.4ppm and 0.6ppm.

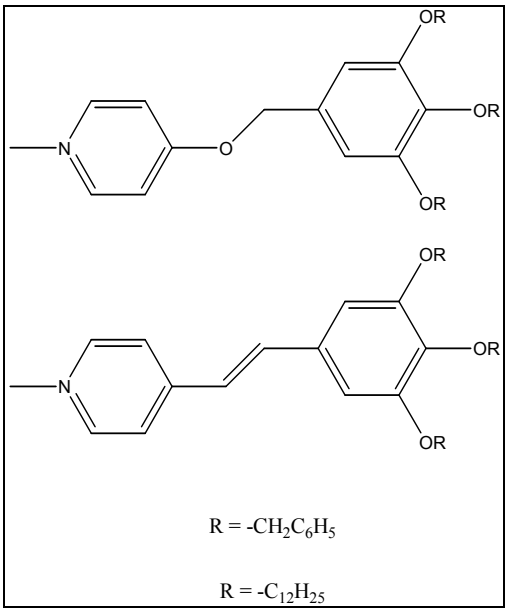


Figure 1.14: Zheng's dendron structures

The difference between the two dendron structures was apparent in the appearance of the recovered products and in the UV-Vis absorption spectra. The ether-based dendrimers were green solids and the alkene-based dendrimers were orange/red solids. The ether-based dendron resulted in the appearance of a band at approximately 630nm, believed to be a ligand to metal charge transfer (LMCT) band. The LMCT band was not present in the alkene dendrimer absorption spectrum. One concern with the absorption data presented was the difference of the concentrations of the different solutions being investigated. The data compared $[Re_6Se_8(MeCN)_6]^{2+}$ and the ether-based dendrimer with 0.5mM concentration, but the alkene-based dendrimer solution was 0.005mM. Some detail in the absorption spectra may have been lost with such a dilute solution and no explanation for the difference in concentration was offered.

The other dendrimers synthesized by Zheng[6] consisted of multiple rhenium-selenide core clusters. These dendrimers were synthesized using 6 equivalents of

$[Re_6Se_8(PEt_3)_5(L)]^{2+}$ and one equivalent of $[Re_6Se_8(MeCN)_6]^{2+}$, where L was a bis-pyridyl linkage shown in **Figure 1.15**. The PEt_3 groups have been previously shown to resist ligand exchange[47, 48], so the design of the $[Re_6Se_8(PEt_3)_5(L)]^{2+}$ clusters allowed for just one possible product to be formed.

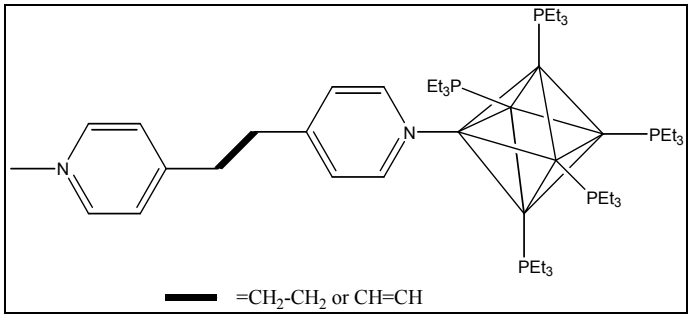


Figure 1.15: Zheng's dendron designed with terminal rhenium-selenide clusters

Ligand exchange was completed in refluxing chlorobenzene for 3 hours. ^{1}H NMR shifts of the pyridyl ring closest to the central rhenium-selenide core were upfield, opposite of the shifts reported in Zheng's previous dendrimer study. This phenomenon may have been due to the presence of the other rhenium-selenide core attached to the pyridyl linkage. Downfield shifts were observed for signals in ^{31}P NMR spectra. ^{77}Se NMR was also used to characterize $[Re_6Se_8(MeCN)_6]^{2+}$, $[Re_6Se_8(PEt_3)_5(L)]^{2+}$, and the resulting dendrimers. The dendron ^{77}Se NMR showed two peaks and there was no shift observed for these peaks following ligand exchange. The dendrimer ^{77}Se NMR exhibited a new peak due to the selenium on the central core cluster. Cyclic voltammetry of these dendrimers showed two oxidation peaks, one at 1.26V and the other at 1.91V. The first peak was reversible, but the second was not. Comparison of the peaks showed a 1:6

ratio, which was consistent with the first peak corresponding to the central core and the second peak corresponding to the six terminal $[Re_6Se_8]^{2+}$. This ratio was consistent with the simultaneous oxidation of the terminal $[Re_6Se_8]^{2+}$ clusters, suggesting that all of the terminal species are equivalent as expected. Both of these peaks were shifted to more positive potentials compared to other rhenium-selenide core molecules.

Summary

Preliminary research on oLEDs by many scientists has led to a desire to design materials with high quantum yields and long emission lifetimes for the emitting layer. The emitting layer should also be able to transport holes and electrons to allow for recombination within the emitting layer, allowing excitation and therefore fluorescence. The ablilty to transfer holes and electrons necessitates redox behavior of the dendrimer core, although the core should exhibit mostly insulating behavior so that the holes and electrons can recombine within the emitting layer.

Frechet and Balzani showed that increasing dendrimer generation resulted in increased quantum yields and emission lifetimes[4, 11, 22, 26]. Moore showed that the dendritic architecture allows for energy transfer from the dendron terminal groups to the dendrimer core[41, 42]. These studies show that dendritic architectures may be designed to enhance the luminescence of a core moiety, making dendrimers a good choice for the emitting layer of oLEDs.

There have been many studies showing that as dendrimer generation increases, the kinetic reversibility decreases[9, 18, 35, 36]. Studies by Gorman comparing different dendrimer architectures, rigid vs. flexible and extended vs. backfolded, have shown that the architecture also has a significant effect on the electron transfer kinetics[9, 16]. These

observations lead to the conclusion that the rate of electron transport can be controlled through dendron design and dendrimer generation.

The photophysical and electrochemical properties of dendrimers offer the ability to fine-tune the properties of a dendrimer core. The dendrimer core will dictate the photophysical and electrochemical properties of a dendrimer. Rhenium-selenide cores exhibit high quantum yields and long lifetimes with many different attached ligands[53, 54]. These cores have also been shown to be redox active by Batail[51].

Zheng has previously synthesized rhenium-selenide core dendrimers[6, 55]. These dendrimers exhibited irreversible electrochemical behavior and no fluorescence experiments were conducted. The poor electrochemical properties of these dendrimers offered the opportunity to explore different dendrimer architectures.

The dendrons explored in this work are poly(benzyl ether) dendrons with cyano focal points. Previous work has shown that these dendrons encapsulate cores, slowing electron transfer rates, and also allow energy transfer[11, 26, 33]. The properties of dendrimers with these dendrons and the luminescent and redox active rhenium-selenide core will be explored in this thesis.

The next chapter will focus on the synthetic procedures for the synthesis of the rhenium-selenide core, poly(benzy ether) dendrons, and ligand exchange resulting in dendrimer formation. The third and fourth chapters will investigate the photophysical and electrochemical properties of zero-, first-, and second-generation dendrimers.

Chapter 1 References

1. Mitschke, U. and P. Bauerle, J. Mater. Chem., 2000: p. 1471-1507.
2. Chen, C.H. and J. Shi, Macromol. Symp., 1997: p. 1-48.
3. Tsutsui, T., MRS Bulletin, 1997: p. 39-45.
4. Vogtle, F., et al., *Dendrimers with a photoactive and redox-active Ru(bpy)(3) (2+)-type core: Photophysical properties, electrochemical behaviour, and excited-state electron-transfer reactions.* Journal of the American Chemical Society, 1999. **121**(26): p. 6290-6298.
5. Venturi, M., et al., *Electrochemical and photochemical properties of metal-containing dendrimers*, in *Dendrimers*. 1998. p. 193-228.
6. Zheng, Z., B.K. Roland, and C. Carter, *Routes to Metallodendrimers of the [Re6(μ3-Se)8]2+ Core-Containing Clusters.* Journal of the American Chemical Society, 2002. **124**: p. 6234-6235.
7. Kaifer, A.E. and W. Ong, *Unusual Electrochemical Properties of Unsymmetric Viologen Dendrimers.* Journal of the American Chemical Society, 2002. **124**: p. 9358-9359.
8. Kaifer, A.E., C.M. Cardona, and S. Mendoza, *Electrochemistry of Encapsulated Redox Centers.* Chemical Society Reviews, 2000. **29**: p. 37-42.
9. Gorman, C.B. and J.C. Smith, *Structure-property relationships in dendritic encapsulation.* Accounts of Chemical Research, 2001. **34**(1): p. 60-71.
10. Gorman, C.B., *Encapsulated electroactive molecules.* Advanced Materials, 1997. **9**(14): p. 1117-1119.
11. Frechet, J.M.J. and A. Adronov, *Light-Harvesting Dendrimers.* Chemical Communications, 2000: p. 1701-1710.
12. Frechet, J.M.J., et al., *Dendrimer-containing light-emitting diodes: Toward site-isolation of chromophores.* Journal of the American Chemical Society, 2000. **122**(49): p. 12385-12386.
13. Diederich, F. and B. Felber, *Supramolecular Chemistry of Dendrimers with Functional Cores.* Proceedings of the National Academy of Sciences of the United States of America, 2002. **99**(8): p. 4778-4781.
14. Balzani, V., et al., *Dendrimers based on electroactive metal complexes. A review of recent advances.* Collection of Czechoslovak Chemical Communications, 2001. **66**(1): p. 1-32.
15. Balzani, V., et al., *Dendrimers based on photoactive metal complexes. Recent advances.* Coordination Chemistry Reviews, 2001. **219**: p. 545-572.
16. Gorman, C.B., et al., *Structural Effects on Encapsulation As Probed in Redox-Active Core Dendrimer Isomers.* Journal of the American Chemical Society, 2003. **125**: p. 8250-8254.
17. Gorman, C.B. and C.S. Cameron, *Effects of site encapsulation on electrochemical behavior of redox-active core dendrimers.* Advanced Functional Materials, 2002. **12**(1): p. 17-20.
18. Gorman, C.B., et al., *Molecular Structure-Property Relationships for Electron-Transfer Rate Attenuation in Redox-Active Core Dendrimers.* Journal of the American Chemical Society, 1999. **121**: p. 9958-9966.

19. Smith, J.C., *Structure-property Relationships for Alternatively Stiff and Flexible Redox-Active Core Dendrimers of the Type, [Fe4S4(S-Dend)4]2-*, in *Chemistry*. 1999, North Carolina State University: Raleigh.
20. Kaifer, A.E. and e. al., *A New Series of Dendrimers with 4-4'-bipyridinium Cores Capable of Fast Electron Transfer Reactions.* Chemical Communications, 2001. **9**: p. 857-858.
21. Balzani, V. and e. al., *Dendrimers with a 4-4'-bipyridinium Core and Electron-Donor Branches. Electrochemical and Spectroscopic Properties.* Advanced Functional Materials, 2001. **25**(8): p. 989-993.
22. Balzani, V., et al., *Supramolecular Dendrimers with a [Ru(bpy)3]2+ Core and Naphthyl Peripheral Units.* New Journal of Chemistry, 1999: p. 63-69.
23. Frechet, J.M.J., S.L. Gilat, and A. Adronov, *Light Harvesting and Energy Transfer in Novel Convergently Constructed Dendrimers.* Angewandte Chemie International Edition in English, 1999. **38**(10): p. 1422-1427.
24. Aida, T., T. Sato, and D.L. Jiang, *A Blue-Luminescent Dendritic Rod: Poly(phenyleneethynylene Within a Light-Harvesting Dendritic Envelope.* Journal of the American Chemical Society, 1999. **121**: p. 10658-10659.
25. Frechet, J.M.J., et al., *Effects of dendrimer Generation on Site Isolation of Core Moieties: Electrochemical and Fluorescence Quenching Studies with Metalloporphyrin Core Dendrimers.* Chemical Materials, 1998. **10**: p. 30-38.
26. Frechet, J.M.J. and M. Kawa, *Self-assembled lanthanide-cored dendrimer complexes: Enhancement of the luminescence properties of lanthanide ions through site-isolation and antenna effects.* Chemistry of Materials, 1998. **10**(1): p. 286-296.
27. Newkome, G.R. and e. al., Journal of Organic Chemistry, 1985. **50**: p. 2003-2004.
28. Tomalia, D.A., et. al, Polymer Journal, 1985. **17**: p. 117-132.
29. Abruna, H.D., J.I. Goldsmith, and K. Takada, *Probing Diffusional Transport in Redox-Active Dendrimers.* Journal of Physical Chemistry, B, 2002. **106**: p. 8504-8513.
30. Kaifer, A.E. and e. al., *Molecular Orientation Effects on the Rates of Heterogeneous Electron Transfer of Unsymmetric Dendrimers.* Journal of the American Chemical Society, 1999. **121**: p. 9756-9757.
31. Frechet, J.M.J. and e. al., *A New Convergent Growth Approach for the Synthesis of Dendritic Macromolecules.* Abstracts of Papers of the American Chemical Society, 1990. **199**: p. 316-ORGN.
32. Frechet, J.M.J., *Dendrimers and supramolecular chemistry.* Proceedings of the National Academy of Sciences of the United States of America, 2002. **99**(8): p. 4782-4787.
33. Hawker, C.J., et al., *The Effect of Macromolecular Architecture in Nanomaterials: A Comparison of Site Isolation in Porphyrin Core Dendrimers and Their Isomeric Linear Analogues.* Journal of the American Chemical Society, 2002. **124**: p. 3926-3938.
34. Gorman, C.B., et al., *Control of electron transport using redox-active core dendrimers.* Macromolecular Symposia, 2000. **156**: p. 61-67.

35. Smith, D.K., D.L. Sone, and P.T. McGrail, *Ferrocene Encapsulated within Symmetric Dendrimers: A Deeper Undersanding of Dendritic Effects on Redox Potential.* Journal of the American Chemical Society, 2001. **124**(5): p. 856-864.
36. Kimura, M., et al., *Dendritic Metallophthalocyanines - Synthesis, Electrochemical Properties, and Catalytic Activities.* Chemistry-a European Journal, 1999. **5**(12): p. 3495-3500.
37. Turro, N.J., et al., *Photoinduced Electron-Transfer Reactions to Probe the Structure of Starburst Dendrimers.* Macromolecules, 1990. **23**: p. 910-912.
38. Frechet, J.M.J. and M. Kawa, *Self-Assembled Lanthanide-Cored Dendrimer Complexes: Enhancement of the Luminescence Properties of Lanthanide Ions Through Site-Isolation and Antenna Effects.* Chemical Materials, 1998. **10**: p. 286-296.
39. Kaifer, A.E., et al., *Dendrimers Functionalized with a Single Fluorescent Dansyl Group Attached "Off Center": Synthesis and Photophysical Studies.* Journal of the American Chemical Society, 2000. **122**(26): p. 6139-6144.
40. Castellano, F.N., X. Zhou, and D.S. Tyson, *First Generation Light-Harvesting Dendrimers with a [Ru(bpy)3]2+ Core and Aryl Ether Ligands Functionalized with Coumarin 450.* Angewandte Chemie International Edition in English, 2000. **39**(23): p. 4301-4305.
41. Moore, J.S., P. Bharathi, and C. Devadoss, *Energy Transfer in Dendritic Macromolecules: Molecular Size Effects and the Role of an Energy Gradient.* Journal of the American Chemical Society, 1996. **118**: p. 9635-9644.
42. Kopelman, R., et al., *Dendrimer photoantenna supermolecules: Energetic funnels, exciton hopping, and unusual excimer formation.* Abstracts of Papers of the American Chemical Society, 1999. **218**: p. 17-PHYS.
43. Fedorov, V.E., A.A. Opalovski, and E.U. Lobkov, Russian Journal of Inorganic Chemistry, 1971. **16**: p. 790.
44. Leduc, L., A. Perrin, and M. Sergent, *Structure of Hexarhenium octaselenide dichloride, Re6Se8Cl2: Bidimensional Compound with Re6 Octahedaral Clusters.* Acta Crystallographica, Section C: Crystal Structure Communications, 1983. **C39**(11): p. 1503-1506.
45. Holm, R.H., J.R. Long, and L.S. McCarty, *A Solid-State Route to Molecular Clusters: Access to the Solution Chemistry of [Re6Se8]2+ (Q=S,Se) Core-Containing Clusters via Dimensional Reduction.* Journal of the American Chemical Society, 1996. **118**: p. 4603-4616.
46. Holm, R.H., Z. Zheng, and J.R. Long, *A Basis Set of Re6Se8 Cluster Building Blocks and Demonstration of Their Linking Capability: Directed Synthesis of Re12Se16 Dicluster.* Journal of the American Chemical Society, 1997. **119**: p. 2163-2171.
47. Holm, R.H. and Z.P. Zheng, *Cluster condensation by thermolysis: Synthesis of a rhomb- linked Re12Se16 dicluster and factors relevant to the formation of the Re24Se32 tetracluster.* Inorganic Chemistry, 1997. **36**(23): p. 5173-5178.
48. Holm, R.H., Z.P. Zheng, and J.R. Long, *A basis set of Re6Se8 cluster building blocks and demonstration of their linking capability: Directed synthesis of an Re12Se16 dicluster.* Journal of the American Chemical Society, 1997. **119**(9): p. 2163-2171.

49. Holm, R.H., et al., *Ligand substitution reactions of Re6S8Br6 (4-): A basis set of Re6S8 clusters for building multicluster assemblies.* Inorganic Chemistry, 1998. **37**(2): p. 328-333.
50. Holm, R.H., Z.P. Zheng, and T.G. Gray, *Synthesis and structures of solvated monoclusters and bridged di- and triclusters based on the cubic building block Re- 6(mu(3)-Se)(8) (2+).* Inorganic Chemistry, 1999. **38**(21): p. 4888-4895.
51. Batail, P., et al., *Chemistry of Hexanuclear Rhenium Chalcohalide Clusters.* Chemical Reviews, 2001. **101**: p. 2037-2066.
52. Hughbanks, T. and R. Hoffman, *Molybdenum chalcogenide: clusters, chains, and extended solids. The approach to bonding in three dimensions.* Journal of the American Chemical Society, 1983. **105**: p. 1150-1162.
53. Gray, T.G., et al., *Highly emissive hexanuclear rhenium(III) clusters containing the cubic cores Re6S8 (2+) and Re6Se8 (2+).* Inorganic Chemistry, 1999. **38**(26): p. 5932-+.
54. Gray, T.G., et al., *Spectroscopic and Photophysical Properties of Hexanuclear Rhenium (III) Chalcogenide Cluster.* Journal of the American Chemical Society, 2003. **125**: p. 4755-4770.
55. Zheng, Z.P. and R.Y. Wang, *Dendrimers supported by the Re6Se8 (2+) metal cluster core.* Journal of the American Chemical Society, 1999. **121**(14): p. 3549-3550.

Chapter 2 : Synthesis

Introduction

This chapter will highlight the synthesis of $[Re_6Se_8(CH_3CN)_6](SbF_6)_2$, first and second generation poly(benzyl ether) dendrons, and ligand exchange resulting in dendrimer formation. The synthesis of both $[Re_6Se_8(CH_3CN)_6](SbF_6)_2$, the dendron core, and the poly(benzyl ether) dendrons are based on literature precedence[1-9]. Ligand exchange was require less rigorous conditions then other rhenium-selenide core dendrimers[10, 11].

Core Synthesis

The core synthesis required three steps, previously reported by Holm[1, 2]. The synthesis is shown below in **Figure 2.1**.

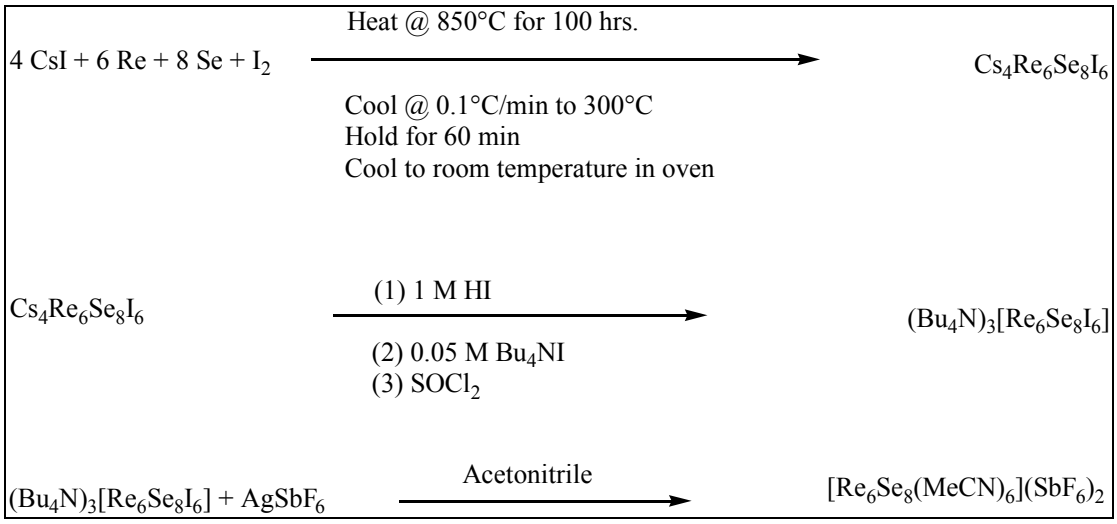


Figure 2.1: Three-step synthesis of rhenium-selenide core

The synthesis of $Cs_4Re_6Se_8I_6$ began with the attachment of thick-walled quartz tubing to a vacuum top. The tube, three spatulas, and a mortar and pestle were pumped into a dry box. The tube was filled with stoichiometric amounts of rhenium powder and crushed selenium. Two extra equivalents of cesium iodide were added to the tube and then the tube was closed to the atmosphere. The tube was removed from the dry box and placed under vacuum with the bottom of the tube submerged in liquid nitrogen such that the reactants were below the liquid nitrogen level. The tube remained under vacuum for 10 minutes before back-filling with nitrogen for 2-3 minutes. This process was repeated two more times. While filling with nitrogen for the final time iodine, 10% excess by weight was added to the tube. The top of the tube was replaced and the tube was placed under vacuum. The tube was then sealed using a hydrogen torch, creating a tube as short as possible. The sealed tube was allowed to warm to room temperature in the hood before moving it to the oven.

A diagram of the oven is shown in **figure 2.2**. The temperature range was found to be 10°C between the center and the end of the oven. The reactants were situated at the cool end of the oven and the tip of the thermocouple was placed at the middle of the tube. The oven program was designed to heat at 2°C/min, hold for 6000 minutes, cool at 0.5°C/min to 300°C. The oven was allowed to cool to room temperature before removing the tube.

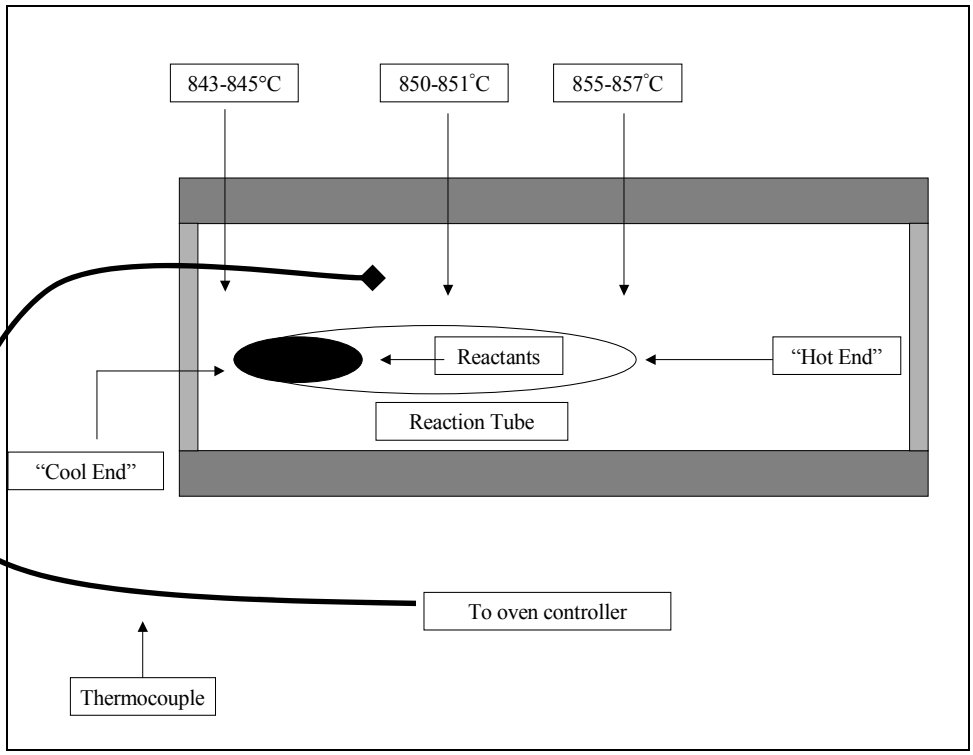


Figure 2.2: Oven Diagram

The recovered product was a red solid. The presence of a black solid was the result of the formation of $CsRe_6Se_8I_3$. This product is formed under the same reaction conditions, but with the appropriate stoichiometric amounts. Excess cesium iodide was recovered as a white solid.

Dry boxes containing sulfur-containing compounds must be avoided due to the possibility of reaction with rhenium. The cesium iodide must be dried for 2 days at 250°C before entering the dry box atmosphere. The cesium iodide is crucial to the reaction mixture and the two extra equivalents were necessary to consistently recover the desired product.

The $Cs_4Re_6Se_8I_6$ product was ground to a fine powder for the synthesis of $(Bu_4N)_3[Re_6Se_8I_6]$. Hydriodic acid was extracted with tributyl phosphate in chloroform (50/50 by volume) until colorless[12] and then diluted to 1M. The crushed $Cs_4Re_6Se_8I_6$

and the colorless hydriodic acid were added to a round bottom flask covered in tinfoil. The solution was stirred in the absence of light for two hours. A saturated, aqueous solution containing 4.5 equivalents Bu_4NI was prepared prior to the end of the two-hour stirring period. The hydriodic acid solution was then filtered through a celite plug approximately 10cm high. The Bu_4NI solution was added to the filtrate while stirring. A precipitate formed immediately and was collected via vacuum filtration. This reddich solid was washed with boiling water, 1L per 2 grams. The solid was dissolved in acetonitrile and stirred while 10 drops of thionyl chloride were added. After 15 minutes of stirring, the solution was reduced to dryness leaving a black sticky solid. The solid was washed with ether until the washes were colorless. Crystallization was completed using acetone and toluene, 75:25. Crystallization was very slow, in one case over a month. The recovered hexagonal crystals were black and small. Slower crystallization did not result in larger crystals.

The purification of hydriodic acid in this step was necessary due to the inability to obtain colorless acid from all manufacturers investigated. It was determined that hydriodic stabilized with hypophosphorous acid was available as a colorless liquid and would not interfere with the reaction[13]. Hydriodic acid is light sensitive and was therefore purified immediately prior to the reaction and stirred in the absence of light to delay degradation. Use of colored hydriodic acid resulted in the formation of an oil. Filtration through celite removed the unreacted rhenium and selenium from the tube reaction. The boiling water wash removed unreacted Bu_4NI and thionyl chloride was used to remove any remaining water. Uncrystallized product often remained sticky and was difficult handle.

For the final step in core formation $(Bu_4N)_3[Re_6Se_8I_6]$ and $AgSbF_6$ were added to a round bottom flask in darkness. The flask was covered in tinfoil and a 50/50 mixture of methylene chloride and acetonitrile was added. The solution was stirred overnight in the absence of light. The solution was then exposed to a sun lamp for 2 hours. The solution was reduced to dryness, then dissolved in a large excess of methylene chloride and filtered through celite. The resulting yellow-orange solution was reduced to a volume of approximately 10mL and allowed to crystallize, forming needle-like orange-yellow crystals.

Recovered crystals were characterized by ^1H NMR. **Figure 2.3** shows two different spectra of $[Re_6Se_8(CH_3CN)_6](SbF_6)_2$. The spectrum on the left shows multiple peaks around the expected singlet at 2.695ppm.

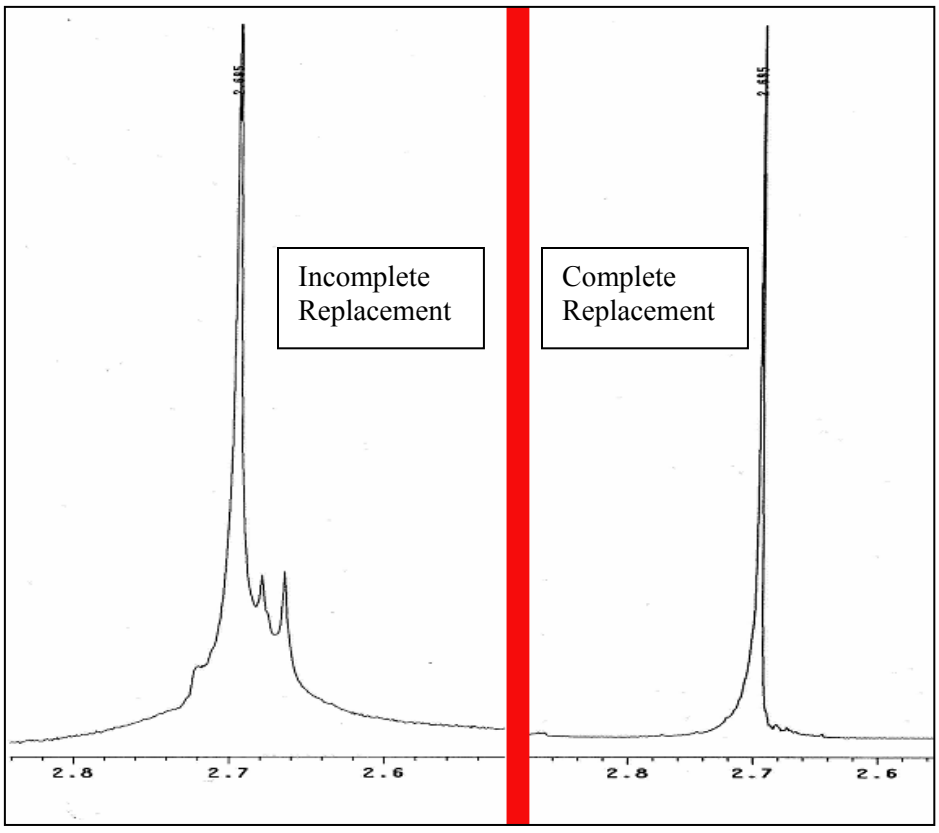


Figure 2.3: ^{1}H NMR of $[Re_6Se_8(CH_3CN)_6](SbF_6)_2$

The multiple peaks were hypothesized to be due to incomplete replacement of iodine by acetonitrile. Exposure of this mixture to reaction conditions resulted in the spectrum on the right, exhibiting one singlet at 2.695ppm.

Attempts at recrystallization in methylene chloride were unsuccessful as the product is no longer soluble in methylene chloride at room temperature. The solid was soluble in acetonitrile and recrystallization attempts produce similar crystals. Material insoluble in acetonitrile was believed to be silver salts and was removed by filtration through celite.

Dendron Synthesis

The poly(benzyl ether) synthesis is well established within the Gorman group[4, 6-8, 14]. The synthesis of the first- and second-generation dendrons used in this study were synthesized by Namjin Kim. The dendron synthesis and dendron structures are shown in **Figure 2.4**.

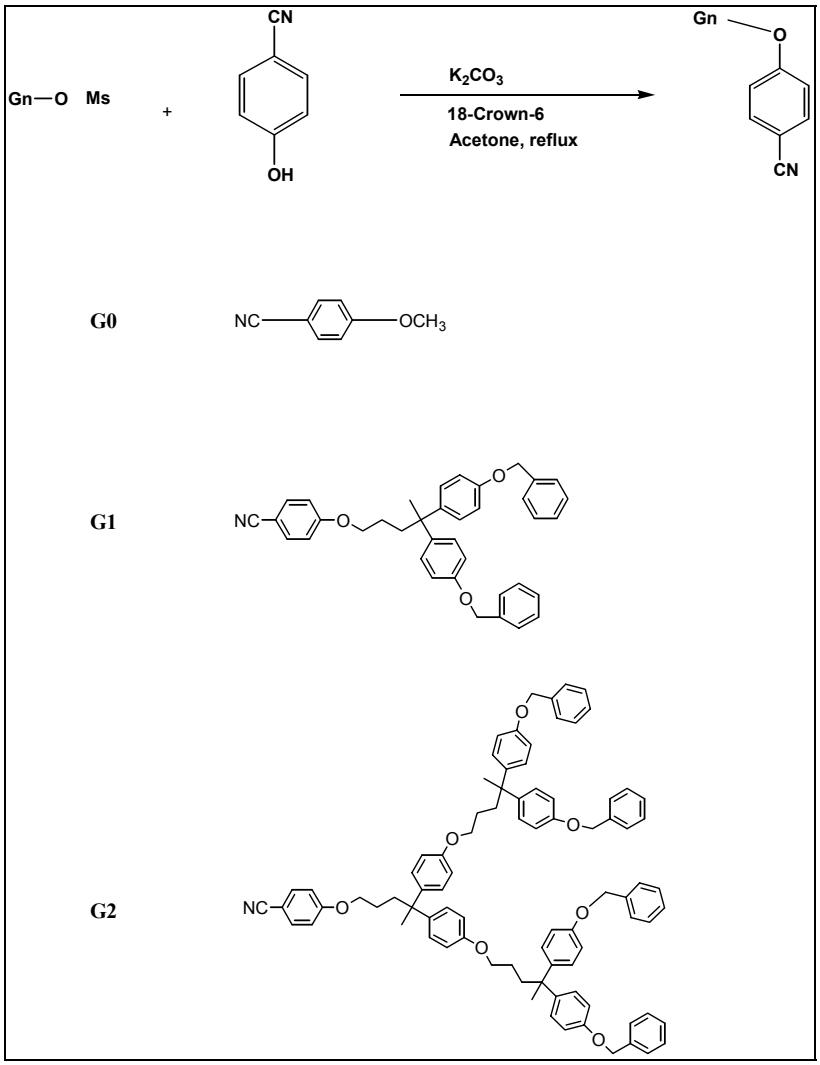


Figure 2.4: Dendron synthesis and structures

The dendrons were recovered as white powders following purification.

Ligand Exchange

Ligand exchange was completed by adding $[Re_6Se_8(CH_3CN)_6](SbF_6)_2$ and 7.5 equivalents of Gx dendron to a round bottom flask. An appropriate volume of 1,2-dichlorobenzene, approximately 5mL per 100mg of $[Re_6Se_8(CH_3CN)_6](SbF_6)_2$, was added and the solution stirred under nitrogen at 110°C for 24 hours.

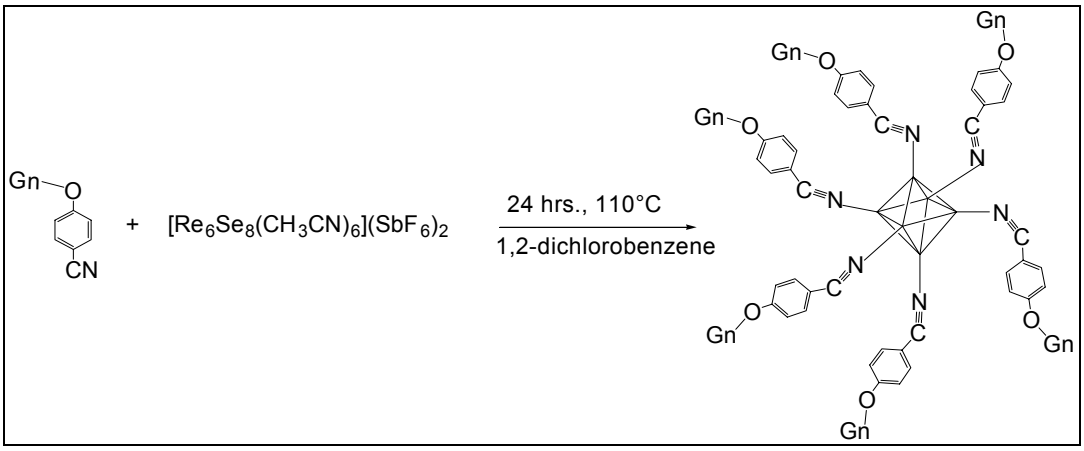


Figure 2.5: Ligand exchange conditions

Reaction completion was assumed when the solution changed from cloudy white to transparent orange. Upon completion the solvent was removed by vacuum at 60°C. The resulting solid was dissolved in 3mL of dry methylene chloride and transferred to two centrifuge tubes. The remaining volume was filled with dry ether, causing the formation of a yellow solid. The tubes were centrifuged for 4 minutes. The liquid was removed and the solids were each dissolved in 1mL of methylene chloride. Approximately 5mL of ether was added to each tube, followed by 4 minutes centrifuging. The liquid was removed and the solid dissolved in 1mL of methylene chloride. Thin layer chromatography was completed using 100% ether as the solvent system. A spot following the solvent front was identified as excess dendron and a spot remaining on the baseline corresponded to the dendrimer. Ether precipitations were continued until no dendron was present. When excess dendron was no longer present, the solution was transferred to a glass vial and the solution was allowed to evaporate off under nitrogen.

Dendrimer formation was characterized by downfield shifts in the ^{1}H NMR. The protons closest to the rhenium-selenide core shifted downfield, similar to the observations of Zheng[10, 11]. The aromatic region of the ^{1}H NMR for the different dendrons and

dendrimers are shown in **Figures 2.6, 2.7, and 2.8**. The downfield shift is easily recognized in the first- and second-generation dendrimers by the presence of a new peak. Incomplete ligand exchange was not encountered.

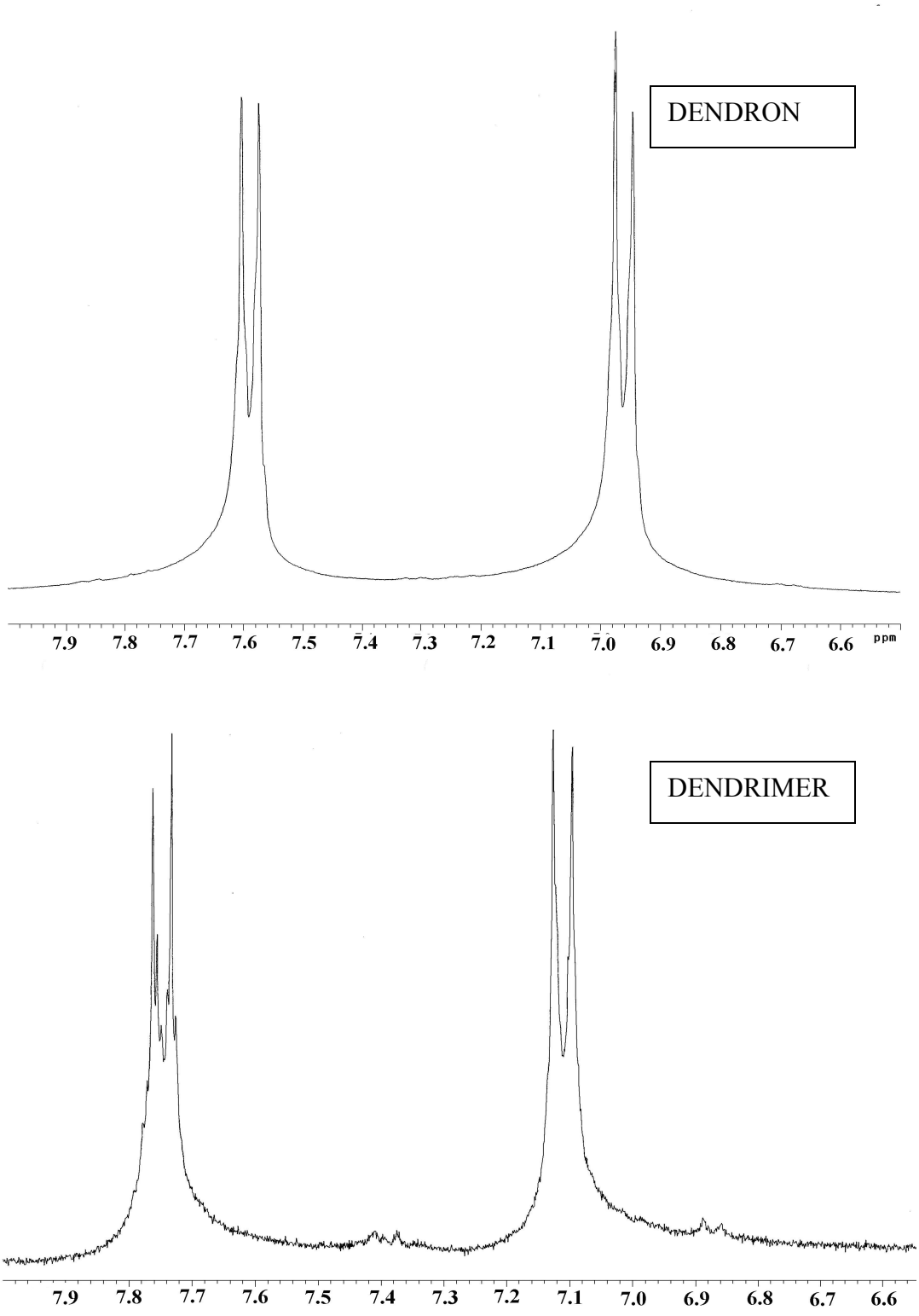


Figure 2.6: G0 ^{1}H NMR

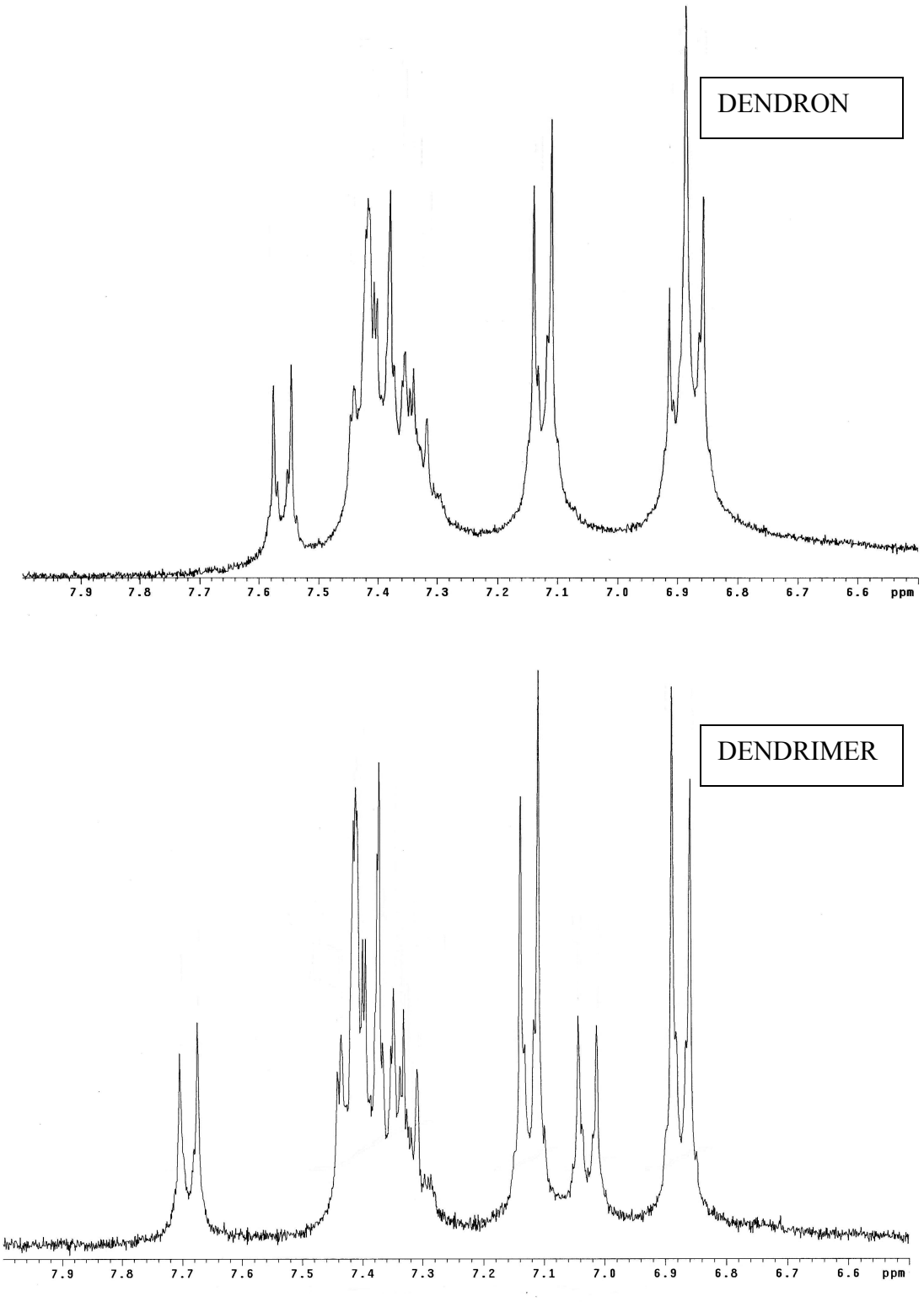


Figure 2.7: G1 ^{1}H NMR

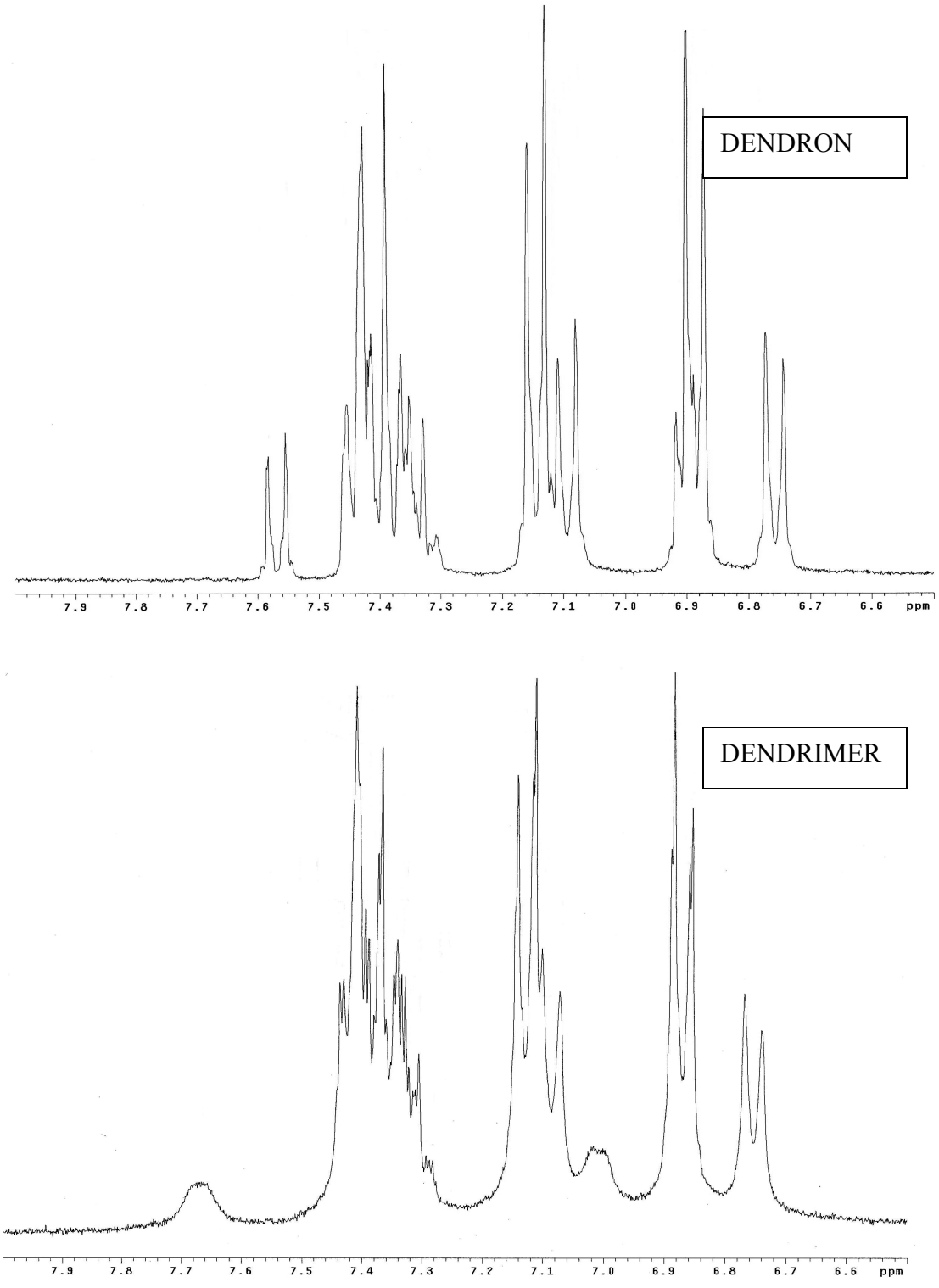


Figure 2.8: G2 ^{1}H NMR

Attempts at dendrimer purification using column chromatography were unsuccessful despite reported success by the Zheng group[13]. Using a 10:1 methylene chloride:acetonitrile resulted in tailing of the dendrimer spot, which was followed very closely by a spot representing the remaining silver salts. Separation of the spots did not increase with any solvent system alterations. Attempts at a flash column and a gravity column resulted in no product being recovered. The product was observed still on the silica of the gravity column despite washes with 100% methylene chloride.

It was determined that crystallization must be done under nitrogen to ensure product integrity. Crystallizations done not under nitrogen resulted in some insoluble material remaining when dissolving the crystals in methylene chloride. Filtration through celite, followed by recrystallization, and addition of methylene chloride would resulted in the presence of more insoluble material. The dendrimers also exhibited a decrease in emission intensity when kept in solution. The mechanism of decomposition and the resulting products were not investigated.

Conclusion

The formation of $[Re_6Se_8(CH_3CN)_6](SbF_6)_2$ required some deviation from published literature in order to maximize yield. Dendron synthesis was straight forward following the choice of the cyano focal point. The synthesis of rhenium-selenide core dendrimers has been completed using less rigorous conditions then previously reported[10, 11]. These rhenium-selenide core dendrimers have been characterized using a variety of techniques and were carried on to photophysical and electrochemical investigations.

Experimental

General Considerations. All reagents were used as received unless otherwise noted. Rhenium, selenium, and cesium iodide were purchased from Aldrich. Rhenium was purchased as 100 mesh and selenium was purchased as pellets, <4mm. Cesium iodide was dried for two days at 250ºC before entering dry box. Hydriodic acid was purchased unstabilized as either 55%-57% or 47% and then diluted according to the certificate of analysis concentration. Colored hydriodic acid was extracted with tributyl phosphate in chloroform until transparent prior to use. 4-cyanobenzene was purchased from Aldrich.

$Cs_4Re_6Se_8I_6$. Rhenium, crushed selenium, and cesium iodide were added to a quartz tube in a dry box in the ratio 6:8:6. The tube was then sealed to the atmosphere and removed from the box. The tube was placed under vacuum for 10 minutes, then back-filled with nitrogen for 2 minutes with the reactants submerged in liquid nitrogen. This process was repeated three times. Under positive pressure of nitrogen, one equivalent of iodine was added to the tube. The tube was placed under vacuum and sealed with a hydrogen torch, such that the reaction tube was as short as possible. The tube was allowed to cool and then placed in an oven with the reactants at the cool end of the oven. The tube was heated at 2ºC/min to 850ºC for 6000 minutes, and then cooled at 0.2ºC/min to 300ºC. The oven was then allowed to cool to room temperature at its own rate. The product was removed from the tube as a red solid.

$(Bu_4N)_4[Re_6Se_8I_6]$. 2g (0.657mmol) $Cs_4Re_6Se_8I_6$ was crushed and then stirred in 200mL of 1M hydriodic acid for 2 hours in the absence of light. The solution was filtered

through celite yielding a red solution. A saturated aqueous solution containing 1.025g (2.775mmol, 4.2equiv.) of $(Bu_4N)I$ was then added to the filtrate. A reddish/black precipitate formed immediately. The solid was collected by filtration and then washed with 1L of boiling water. The solid was dissolved in acetonitrile and 10 drops of thionyl chloride was added and the solution stirred for 15 minutes. The solution was reduced to dryness and the resulting solid was washed with ether until washes were colorless. The solid was dissolved in 200mL of acetone and filtered through celite. The filtrate was transferred to a 250mL beaker and 50mL of toluene was added. The beaker was covered with a watch glass. Black crystals were collected by filtration after 10 days. The crystals were washed with water and toluene then dried under vacuum for 12 hours. Yield: 75%. ^1H NMR ($CDCl_3$) δ (ppm): 0.966(t), 1.58(m), 1.94(t), 3.07(t). Elemental analysis calculated for $(C_{48}H_{108}N_3)[Re_6Se_8I_6]$: calculated: C 17.82%, H 3.34%, N 1.30%; Found: C 18.13%, H 3.27%, N 1.22%.

$[Re_6Se_8(CH_3CN)_6](SbF_6)_2$. 0.2g (0.0614mmol) $(Bu_4N)_4[Re_6Se_8I_6]$ and 0.15g (0.4365mmol, 7.1equiv.) of $AgSbF_6$ were dissolved in 25mL of methylene chloride/acetonitrile (1:1 by volume). The solution was stirred in the absence of light for 12 hours. The solution was then stirred for 2 hours in the presence of light. The solution was reduced to dryness. The resulting solid was then redissolved in 50mL of methylene chloride. This solution was filtered through celite. The solution was reduced to dryness, dissolved in methylene chloride, and filtered through celite again. The solvent was allowed to evaporate slowly and the resulting solid was washed with THF. The solid product was collected by vacuum filtration. The solid was dissolved in a couple of drops

of acetonitrile and then diluted to 20mL with methylene chloride. This solution was allowed to evaporate slowly, yielding the desired product. The product was recovered as orange needle-like crystals. Yield: 50%. ^{1}H NMR (CD_3CN) δ (ppm): 2.69(s)

$C_{38}H_{35}NO_3$ (G1 dendron). 0.5345g (1.007mmol) G1-Oms, 0.1268g (1.0645mmol) 4-hydroxycyanobenzene, 1.7019g (12.314mmol) K_2CO_3, and 0.05 equivalent of 18-crown-6 were added to a round bottom flask. 40mL of acetone were added and the solution was refluxed overnight under N_2. The solution was cooled to room temperature and the solvent was removed. The remaining solid was dissolved in 20mL of methylene chloride. 20mL of deionized H_2O was added and the organic layer was collected. Extraction with methylene chloride was repeated three times on the aqueous layer. The organic layer was dried with $MgSO_4$. The product was a white solid.

$[Re_6Se_8(C_8H_7NO)_6](SbF_6)_2$ (G0 dendrimer). 0.1353g (0.0562mmol) $[Re_6Se_8(CH_3CN)_6](SbF_6)_2$ was combined with 0.0582g (0.437mmol, 7.78equiv.) 4-cyanobenzene and dissolved in 6mL of dry 1,2-dichlorobenzene. The mixture was heated under N_2 at 110ºC overnight. The solvent was removed by vacuum at 60ºC. The residue was dissolved in methylene chloride. The residue was precipitated with diethyl ether and the solid was collected. Ether precipitation was repeated until only one spot on thin layer chromatography (ether) was observed on the baseline. The solution was then filtered through a celite plug. The solvent was allowed to evaporate off under nitrogen yielding a red/orange solid. Yield: 71%. ^{1}H NMR ($CDCl_3$) δ (ppm): 3.92(s, 18H), 7.12(d, 12H, J=8.8Hz), 7.76(m, 12H). MALDI(m/z): calculated = 1273.46, found = 1273.83.

Elemental Analysis calculated for $Re_6Se_8C_{48}H_{42}O_6N_6Sb_2F_{12}$: Calculated: C 19.08%, H 1.39%, N 2.78%; Found: C 18.23%, H 1.38%, N 2.79%.

$[Re_6Se_8(C_{38}H_{35}NO_3)_6](SbF_6)_2$ (G1 dendrimer). 0.1182g (0.0491mmol) $[Re_6Se_8(CH_3CN)_6](SbF_6)_2$ was combined with 0.2113g (0.382mmol, 7.78equiv.) $C_{38}H_{35}NO_3$ and dissolved in 6mL of dry 1,2-dichlorobenzene. The mixture was heated under N_2 at 110ºC overnight. The solvent was removed by vacuum at 60ºC. The residue was dissolved in methylene chloride. The residue was precipitated with diethyl ether and the solid was collected. Ether precipitation was repeated until only one spot on thin layer chromatography (ether) was observed on the baseline. The solution was then filtered through a celite plug. The solvent was allowed to evaporate off under nitrogen yielding a red/orange solid. Yield: 40%. ^{1}H NMR ($CDCl_3$) δ (ppm): 1.54(m, 12H), 1.62(s, 18H), 2.12(br, 12H), 2.21(m, 12H), 4.01(t, 12H, J=6.0Hz), 5.03(s, 24H), 6.89(d, 24H, J=8.8Hz), 7.04(d, 12H, J=9.2Hz) 7.14(d, 24H, J=8.8Hz), 7.30-7.43(m, 60H), 7.70(d, 12H, J=8.8Hz). MALDI(m/z): calculated = 2535.53; found = 2536.83. Elemental Analysis calculated for $Re_6Se_8C_{228}H_{210}O_{18}N_6Sb_2F_{12}$: Calculated: C 49.36%, H 3.79%, N 1.52%; Found: C 49.46%, H 3.89%, N 1.63%.

$[Re_6Se_8(C_{85}H_{81}NO_7)_6](SbF_6)_2$ (G2 dendrimer). 0.1300g (0.054mmol) $[Re_6Se_8(CH_3CN)_6](SbF_6)_2$ was combined with 0.4839g (0.394mmol, 7.30equiv.) $C_{85}H_{81}NO_7$ and dissolved in 6mL of dry 1,2-dichlorobenzene. The mixture was heated under N_2 at 110ºC overnight. The solvent was removed by vacuum at 60ºC. The residue was dissolved in methylene chloride. The residue was precipitated with diethyl ether and

the solid was collected. Ether precipitation was repeated until only one spot on thin layer chromatography (ether) was observed on the baseline. The solution was then filtered through a celite plug. The solvent was allowed to evaporate off under nitrogen yielding a red/orange solid. Yield: 46%. ^{1}H NMR ($CDCl_2$) δ (ppm): 1.59(br, 90H), 2.17(br, 36H), 3.85(br, 24H), 3.96(br, 12H), 5.00(s, 48H), 6.75(d, 24H, J=7.6Hz), 6.86(m, 48H), 6.98-7.12(m, 24H), 7.29-7.41(m, 120H), 7.66(d, 12H, J=8.8Hz). MALDI(m/z): calculated = 4597.46; found = 4603.40. Elemental Analysis calculated for $Re_6Se_8C_{516}H_{498}O_{42}N_6Sb_2F_{12}$: Calculated: C 63.80%, H 5.07%, N 0.88%; Found: C 67.07%, H 5.69%.

Chapter 2 References

1. Holm, R.H., J.R. Long, and L.S. McCarty, *A Solid-State Route to Molecular Clusters: Access to the Solution Chemistry of [Re6Se8]2+ (Q=S,Se) Core-Containing Clusters via Dimensional Reduction.* Journal of the American Chemical Society, 1996. **118**: p. 4603-4616.
2. Holm, R.H. and Z.P. Zheng, *Cluster condensation by thermolysis: Synthesis of a rhomb- linked Re12Se16 dicluster and factors relevant to the formation of the Re24Se32 tetracluster.* Inorganic Chemistry, 1997. **36**(23): p. 5173-5178.
3. Gorman, C.B., et al., *Inorganic core dendrimers as encapsulated electroactive objects.* Abstracts of Papers of the American Chemical Society, 1998. **215**: p. 513-INOR.
4. Gorman, C.B., et al., *Molecular Structure-Propert Relationships for Electron-Transfer Rate Attenuation in Redox-Active Core Dendrimers.* Journal of the American Chemical Society, 1999. **121**: p. 9958-9966.
5. Gorman, C.B., et al., *Control of electron transport using redox-active core dendrimers.* Macromolecular Symposia, 2000. **156**: p. 61-67.
6. Gorman, C.B. and J.C. Smith, *Structure-property relationships in dendritic encapsulation.* Accounts of Chemical Research, 2001. **34**(1): p. 60-71.
7. Gorman, C.B. and C.S. Cameron, *Effects of site encapsulation on electrochemical behavior of redox-active core dendrimers.* Advanced Functional Materials, 2002. **12**(1): p. 17-20.
8. Gorman, C.B., et al., *Structural Effects on Encapsulation As Probed in Redox-Active Core Dendrimer Isomers.* Journal of the American Chemical Society, 2003. **125**: p. 8250-8254.
9. Smith, J.C., *Structure-property Relationships for Alternatively Stiff and Flexible Redox-Active Core Dendrimers of the Type, [Fe4S4(S-Dend)4]2-*, in *Chemistry*. 1999, North Carolina State University: Raleigh.
10. Zheng, Z., B.K. Roland, and C. Carter, *Routes to Metallodendrimers of the [Re6(μ3-Se)8]2+ Core-Containing Clusters.* Journal of the American Chemical Society, 2002. **124**: p. 6234-6235.
11. Zheng, Z.P. and R.Y. Wang, *Dendrimers supported by the Re6Se8 (2+) metal cluster core.* Journal of the American Chemical Society, 1999. **121**(14): p. 3549-3550.
12. Armarego, W.L.E. and D.D. Perrirn, *Purification of Laboratory Chemicals*. 4 ed. 1996: Butterworth Heinemann.
13. Zheng, Z., *Personal Communication*. 2002.
14. Gorman, C.B., et al., *Hybrid organic-inorganic, hexa-arm dendrimers based on an Mo6Cl8 core.* Chemical Communications, 1999(10): p. 877-878.

Chapter 3 : Photophysical Investigations

Introduction

Rhenium-selenide core dendrimers were investigated because of the photophysical and electrochemical properties that are favorable for the design of a solid-state device with possible application as an organic light-emitting device (oLED). In order to obtain a better understanding of the encapsulation effects of the dendritic architecture around the rhenium-selenide core photophysical properties were investigated in solution before exploring solid-state devices.

It has been shown that the dendritic architecture enhances the luminescent properties of a dendrimer core[1-11]. The dendrons create a physical barrier around the core preventing quenching by small molecules and self-quenching. Enhancement of luminescent properties should increase with each generation due to the increased shielding associated with each generational increase.

Another area of interest was the possibility of energy transfer occurring from the dendrons to the dendrimer core. The number of terminal groups of a dendrimer increases geometrically with each increase in generation. More terminal groups would allow a dendrimer to absorb more energy at higher generations, which would make higher generation dendrimers appealing for energy absorption and transfer. In order to have efficient energy transfer, the dendron must be designed in such a manner that it emits in the range that the dendrimer core absorbs.

The rhenium-selenide core used in this work has exhibited high quantum yields and emission lifetimes[12, 13]. Poly(benzyl ether) dendrons have been shown to encapsulate dendrimer cores and provide efficient energy transfer[2-6, 9, 14]. Rhenium-

selenide core dendrimers should therefore offer the high quantum yields and emission lifetimes that are desirable for organic light emitting devices. The possibility of energy transfer was also investigated for possible application as an organic light emitting device.

Results and Discussion

UV-Vis

The absorption spectra of the rhenium-selenide core dendrimers were dominated by the absorption of the six dendrons. The absorption spectra of all dendrimers exhibited two large peaks between 200nm-300nm, similar to the absorption spectra of the dendrons themselves.

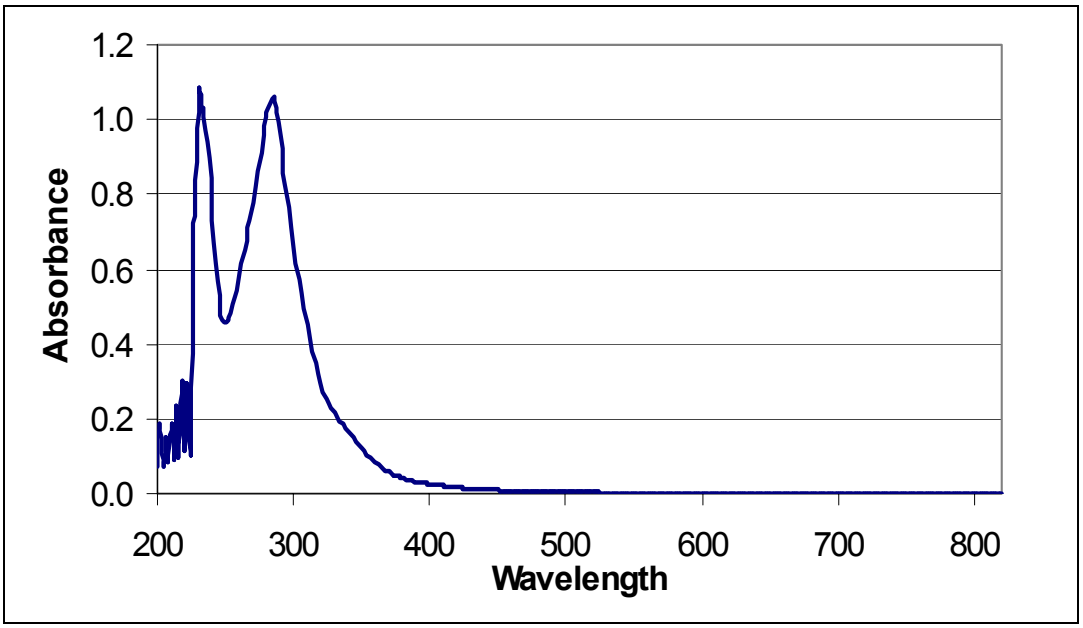


Figure 3.1: UV-Vis absorbance of G1 dendrimer in methylene chloride

Extinction coefficient calculations for the different dendrimers resulted in inconsistent values. The values are shown in **Figure 3.2**. The data shows no specific

trend between concentrations and repeated experiments had similar results. The extinction coefficients for the different dendrimers should be the same at 436nm if the absorption was due to just the rhenium-selenide core. More investigation of the extinction coefficients is necessary to understand the observed phenomenons.

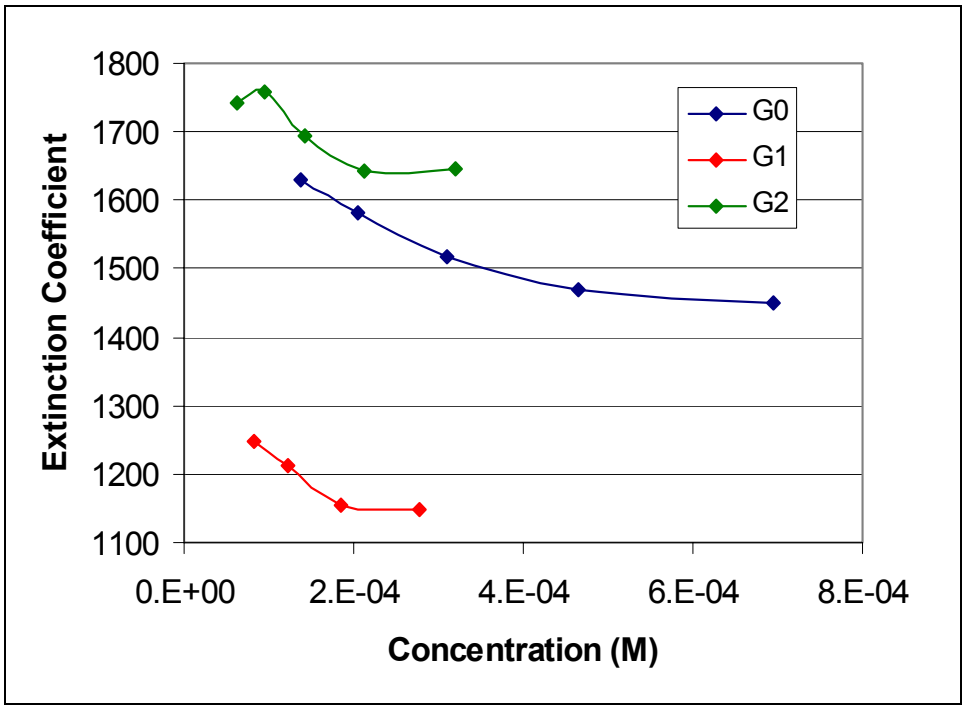


Figure 3.2: Extinction Coefficients for Various Concentrations

The air stability of sample solutions was a concern following difficulties encounter during synthesis and information from fluorescence measurements. There were no changes in the absorption spectra observed during measurements or over time. Solid samples were recovered from absorbance solutions by removal of solvent under nitrogen, which ensured the fluorescence integrity of the recovered product.

Quantum Yield

The choice of 436nm as the excitation wavelength for these studies was based on previous photophysical studies by Gray[12, 13]. The choice was further justified by the absorbance of similar $[Re_6Se_8]^{2+}$ molecules and the fact that 436nm is a strong lamp line. The use of a strong lamp line was preferred because its absolute intensity should not vary much over time.

The quantum yields of the different dendrimers are shown in **Table 3.1**. There was only a slight difference in quantum yield between the dendrimer generations. These results were similar to those of Vogtle[5], where differences in the emission lifetimes of ruthenium core dendrimers were only noticeable in aerated solutions. The small difference between generations may also have been within experimental error, but there were only a few samples available for measurement and therefore experimental errors were not calculated.

Table 3.1: Quantum yield values of rhenium-selenide core dendrimers

Dendrimer	Quantum Yield
G0	0.08
G1	0.09
G2	0.09

These quantum yield experiments differed from previous literature studies because of the decrease in quantum yield from the model molecule to the different dendrimers. The rhenium-selenide core dendrimers exhibited a decrease of approximately 0.01-0.02 from the $[Re_6Se_8(CH_3CN)_6]^{2+}$ actinometer. It was possible that

the dendrons had a stronger interaction with the core, which according to the studies by Gray[12, 13] should result in a decrease in the quantum yield.

Self-quenching was avoided in these experiments by using dilute samples. It is believed that the samples with an absorbance of 0.1 at 436nm were concentrated enough to show self-quenching, but there was no significant change in quantum yield observed between the 0.1 absorbance unit samples and more dilute samples. A more concentrated solution should be investigated to conclude if self-quenching is being prevented. Quenching due to oxygen was also not investigated during these experiments, although this may be investigated in future experiments. Oxygen quenching was avoided in these experiments by completing freeze-pump-thaw cycles. To observe the effect of oxygen quenching, future experiments could be performed to compare aerated solutions to oxygen-free samples.

Investigations concerning the air and solution stability of rhenium-selenide dendrimers were investigated following problems during synthesis. To investigate the solution stability of the dendrimers fresh solutions were compared with day-old solutions. Freshly synthesized G0 dendrimer and previously synthesized G2 dendrimer were used to prepare fluorescence samples with abosorbances of 0.1 at 436nm. Following data collection, the G0 solution was allowed to evaporate off under nitrogen and the G2 sample was kept in solution under a Teflon cap to prevent solvent evaporation. After 24 hours the G0 sample was redissolved in the appropriate amount of solvent necessary to achieve an absorbance of 0.1 at 436nm and the G2 sample was checked to ensure no changes in concentration had occurred. Fluorescence spectra were recorded for each sample and compared to the spectra from the day before. The G0 sample showed no

change in emission intensity, however the G2 sample showed a significant decrease in the fluorescent intensity. The two spectra shown in **Figure 3.1** show the fresh solution and the day old solution of G2 dendrimer.

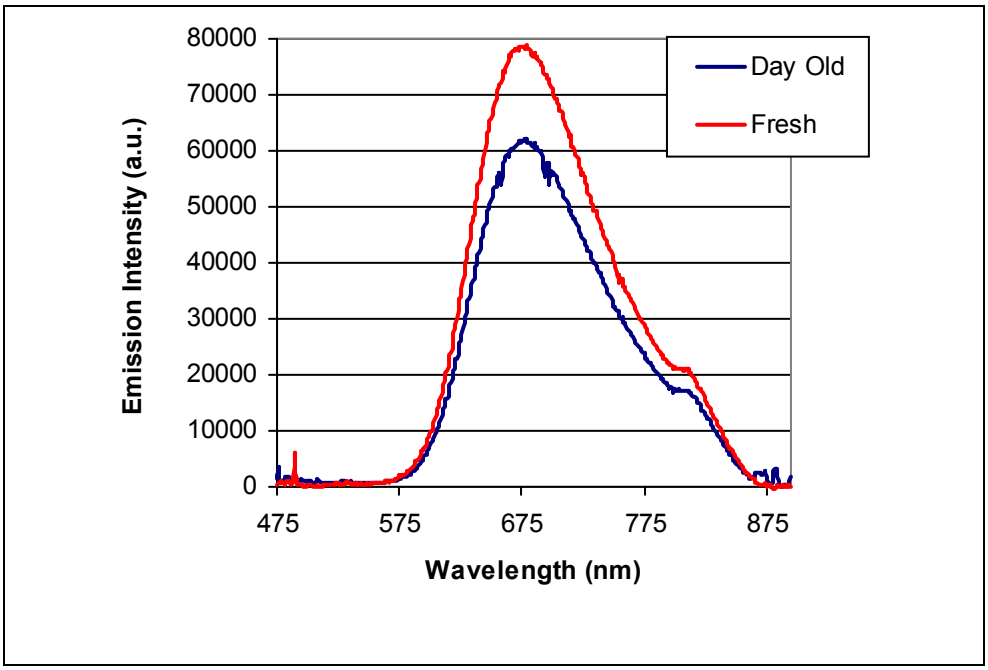


Figure 3.3: Emission spectra of a freshly prepared solution vs. a day-old solution

This study proved that there was some change that occurred if the dendrimer was left in solution for a prolonged period of time. This discovery led to changes mentioned in the synthesis section concerning the crystallization of the dendrimer. All fluorescence studies were repeated with freshly made solutions and the collected data was matched against the spectra collected in this study.

One concern with the stability study was the use of previously prepared G2 dendrimer. When pure $[Re_6Se_8(CH_3CN)_6](SbF_6)_2$ became available, a fresh sample of G2 dendrimer was prepared. The fresh dendrimer was then used to make a solution with

an absorbance of 0.1 at 436nm. The collected spectrum was compared to the spectrum from the earlier study and it was revealed that the fresh solution of previously prepared G2 dendrimer had significantly lower emission intensity. This data led to the realization that the crystallization of the previously prepared G2 had degraded the sample, but more degradation was observed upon further storage as a solution.

The study of the quantum yields of different rhenium-selenide core molecules by Gray[12, 13] showed a possible correlation between the strength of the ligand-rhenium bond and the quantum yield. It appeared that a weaker interaction would result in an increase in the quantum yield. This idea was taken into account when designing the dendrimers used for these studies, but the stability of the dendrimer must also be considered. Although weak bonds may be ideal for fluorescence they may result in the dendrimer decomposing over time. Any future attempts at dendron design with different focal groups will need to account for the need to have a molecule able to withstand the conditions necessary for making a solid-state device. Gray[12, 13] reported that the Re-O and Re-N were the best linkages in their study.

Energy Transfer

Energy transfer experiments were completed to determine the efficiency of energy transfer from the benzyl terminal units to the rhenium-selenide core. The poly(benzy ether) dendrons have previously shown efficient energy transfer to other dendrimer cores[2-6, 9, 14]. Ideal energy transfer can be predicted by overlap of the emission of the donor with the absorbance of the acceptor. Shown in **Figure 3.4** are spectra showing the fluorescence spectrum for G1 dendron and the absorbance spectrum of G1 dendrimer.

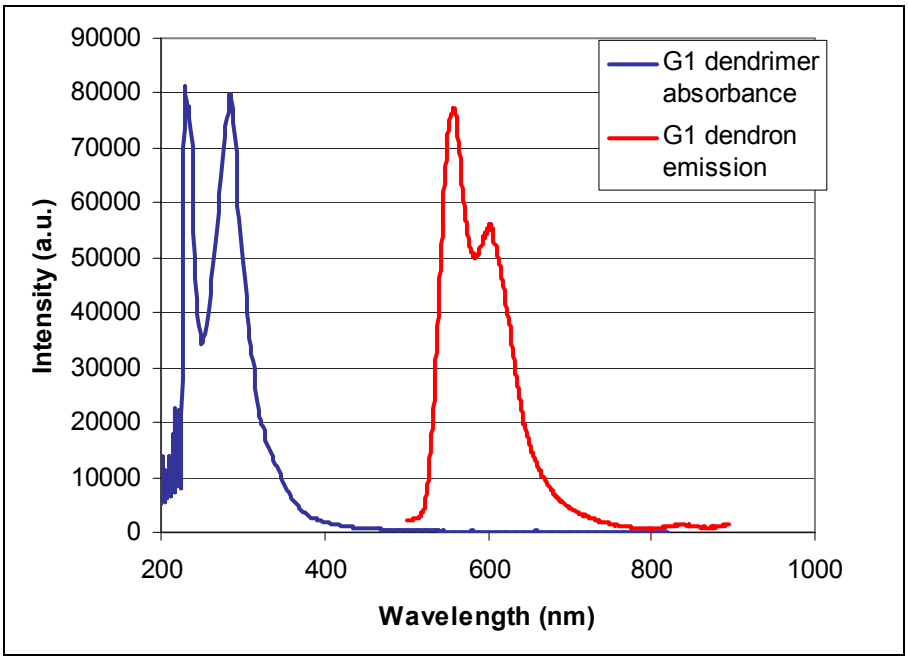


Figure 3.4: G1 dendrimer absorbance and G1 dendron emission

The plot above shows no overlap between the dendron emission and the core absorbance (436nm). The lack of overlap suggested that little to no energy transfer would be expected.

It is believed that energy transfer in dendrimers occurs through space as opposed to through bonds. Förster energy transfer occurs through space and depends on the distance between donor and acceptor. Energy transfer should become less efficient as the distance between the absorbing terminal units become further from the emitting dendrimer core. Therefore energy transfer efficiency should decrease with increasing dendrimer generation. In contrast to this hypothesis is the fact that the number of absorbing terminal groups doubles with each increase in generation. This would suggest that as the dendrimer generation increases, the terminal groups will absorb more energy and therefore more energy would be available to the emitting core.

Energy transfer experiments were completed using 276nm as the excitation wavelength. The excitation wavelength was chosen because of its proximity to the absorption maxima of the dendrons and the strength of the lamp lines in that region. Emission spectra were collected for all dendrons and dendrimers being studied.

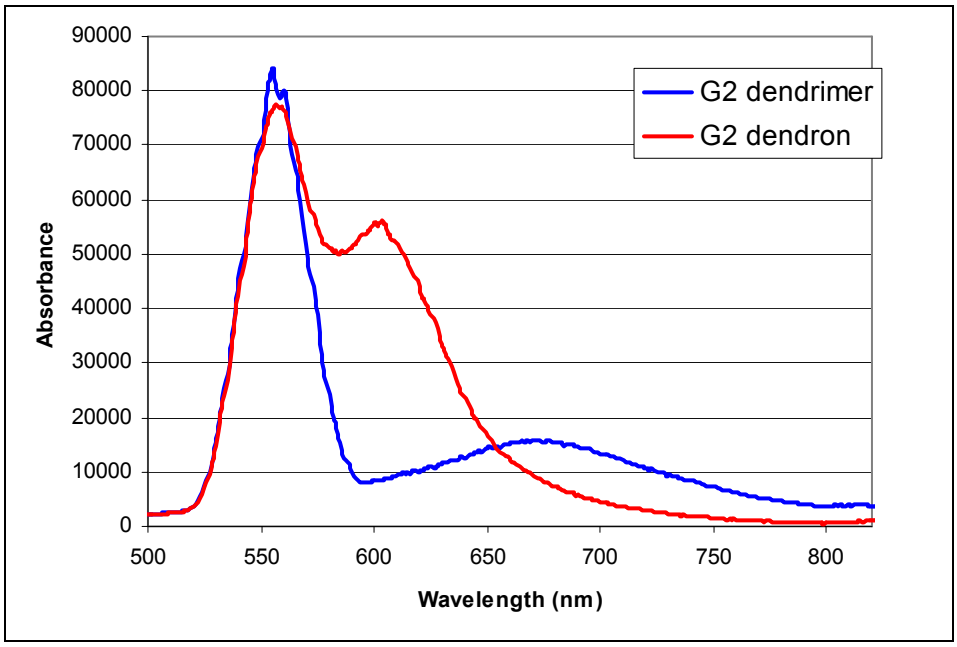


Figure 3.5: Emission spectra of G2 dendron and G2 dendrimer excited at 276nm

The overlay of G2 dendron and G2 dendrimer emission spectra showed the disappearance of the dendron emission peak upon attachment the rhenium-selenide core. The high emission of $[Re_6Se_8(CH_3CN)_6](SbF_6)_2$ was due to the high concentration of the of the emitting $[Re_6Se_8]^{2+}$ core. The concentration was higher then the dendrimer samples because of the low absorbance at 276nm, resulting in a concentrated solution being necessary to achieve an absorbance of 0.1.

The quantification of the amount of energy transfer has been done various ways in the literature. The method employed by Fechet[9] was to show that the entire dendron emission peak disappeared and therefore the core absorbs 100% of the energy emitted by the dendron. An explanation of the energy transfer did not include any information concerning the resulting emission of the core and therefore suggested that all energy was transferred to the core and then emitted by the core. This method did not allow for the possibility of energy loss during the transfer. Using this method, there was 100% energy transfer from the dendrons to the rhenium-selenide core based on the disappearance of the dendron emission peak. This methodology was questioned when comparison of emission spectra of $[Re_6Se_8(G2)_6](SbF_6)_2$dendrimer excited at 436nm and at 276nm showed a large difference in the emission intensity of the core. **Figure 3.4** shows the difference between excitation at 436nm and 276nm.

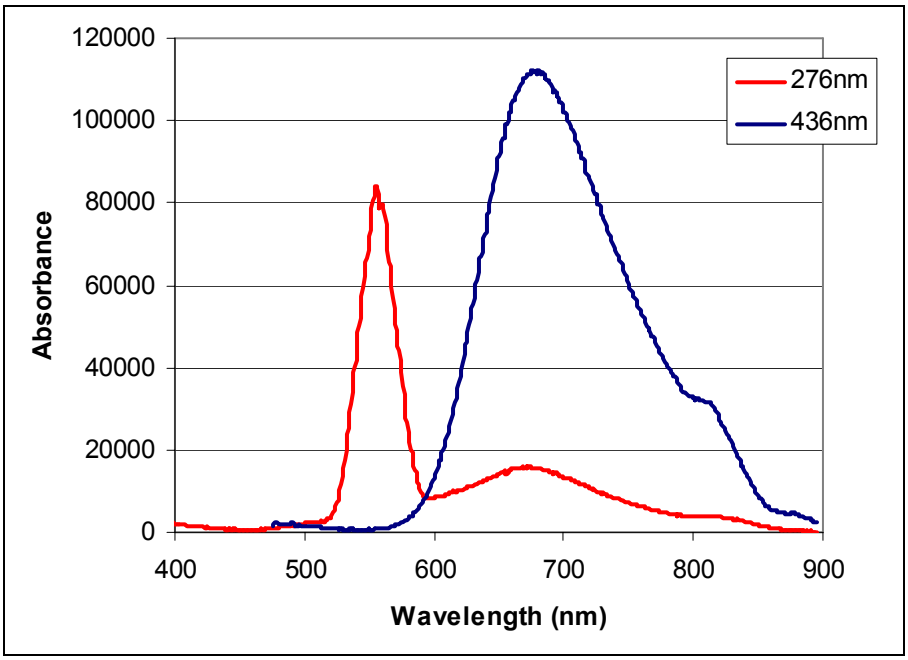


Figure 3.6: Emission spectra of G2 dendrimer when excited at 436nm vs. when excited at 276nm

The difference in emission intensity led to the investigation of another method to quantify the energy transfer[15]. It was hypothesized that comparison of the emission of the core when excited at 436nm to the emission of the core when excited at 276nm may also be a valid method to quantify the energy transfer efficiency. Since the number of photons going into the samples was the same at both excitation wavelengths, the number of photons out should be comparable. A ratio of the emission intensity when exciting at 276nm to the emission intensity when exciting at 436nm was believed to yield the percentage of energy transfer. The flaw with this method is the difference in the number of emitting rhenium-selenide cores between samples. Although the number of photons that go into each sample was the same, solutions excited at 276nm were more dilute then samples excited at 436nm. A more dilute sample should therefore have a lower emission intensity because there are less emitting moieties.

Energy transfer efficiencies were not calculated due to a lack of material and technical problems with the UV-Vis lamp. These values will be calculated when more material becomes available.

Rhenium-selenide core dendrimers were shown to exhibit the good photophysical properties that other rhenium-selenide molecules possess[12, 13]. More work must be done in order to understand the trade-off between good photophysical properties and stability of the dendrimer. These studies should include different dendron architectures and focal points. Studies comparing aerated solutions to air-free solutions of rhenium-selenide dendrimers and $[Re_6Se_8(CH_3CN)_6](SbF_6)_2$ should be completed to identify the encapsulation effects of the dendrons. Quantum yield and emission lifetimes of aerated solutions should be determined and compared to the quantum yield values in deaerated solutions.

Further investigation of energy transfer should focus on the synthesis of a dendron that emits in the 400nm range. The poly(benzyl ether) dendrons exhibited poor energy transfer, but did show that energy transfer was possible.

Experimental

General Considerations. Absorption spectra were recorded using a Hewlett Packard 8452A diode array spectrometer and standard UV-Vis cuvettes with a 10mm pathlength. The instrument was allowed to warm-up for 30 minutes before spectra were recorded. Fluorescence spectra were recorded on an ISS PC1 spectrofluorimeter with a 20-watt ILC illuminator power supply. The power source was set to 18amps and the lamp was allowed to warm-up for one-hour prior to use. Slit widths of 2mm were used and no high or low pass filters were employed. Cuvettes were custom made by the glass scientific

glass shop at North Carolina State University with a vacuum top attached to a quartz sample holder. All four sides of the cuvette were photophysical quality. A mark was made on the neck of the cuvette to ensure that all scans were done using the same face. All samples were ^{1}H NMR pure before being used for photophyiscal experiments. Methylene chloride was used freshly distilled and spectral grade acetonitrile was used as received from Fisher. All dendrimer and dendron solutions were made using methylene chloride. $[Re_6Se_8(CH_3CN)_6](SbF_6)_2$ solutions were prepared using acetonitrile as described in the literature[12].

UV-Vis. Spectra were recorded from 190nm to 820nm. Files were removed from the computer and extinction coefficients were calculated in Microsoft Excel®. Extinction coefficients were calculated using Beer's law:

$$A = \varepsilon \lambda c \tag{3.1}$$

where A is the absorbance, ε is the extinction coefficient, and l is the pathlength. Extinction coefficients were calculated for at least 4 different concentrations for both wavelengths of interest, 276nm and 436nm.

Fluorescence. Sample solutions were made such that the absorbance at the excitation wavelength was equal to 0.1, 0.075, 0.05, and 0.03 absorbance units. Samples were initially prepared with an absorbance of 0.1 at the excitation wavelength and then diluted to the next absorbance level following the fluorescence measurement. Quantum yields were calculated using 436nm as the excitation wavelength. Energy transfer values were calculated using 276nm as the excitation wavelength. Following absorbance

measurements, sample solutions were placed into the fluorescence cuvette and subjected to three freeze-pump-thaw cycles. The sample holder remained closed to the atmosphere and the fluorescence spectrum recorded. To ensure that the concentration of the samples remained unchanged through the freeze-pump-thaw cycles, the absorbance was rechecked following fluorescence measurements.

The quantum yield is the ratio of the number of photons out of a sample to the number of photons into the sample.

$$\Phi = \frac{PhotonsOut}{PhotonsIn} \tag{3.2}$$

Sample solutions were prepared by matching the absorbance of each sample at the excitation wavelength. In order to match the number of photons in, the number of photons absorbed by each sample must be the same and thus the absorbance at the excitation wavelength must be the same. It was important to note that the concentration of the fluorescence samples was not needed for the calculation of quantum yields.

Measuring the number of photons that were emitted from each sample was not possible because of the lack of a photon counting detector. Instead of purchasing a photon counting detector, the use of a molecule with a known quantum yield was employed as an actinometer. An ideal standard is one that emits in the same region as the sample being measured because it eliminates error due to detector variations at different wavelengths. The standard used for these experiments was $[Re_6Se_8(CH_3CN)_6](SbF_6)_2$, which was reported as having a quantum yield of 0.1 in acetonitrile by Gray[12, 13]. The use of this standard was ideal because it emits in the exact same region and was available

due to its use as a precursor to the dendrimers being investigated. The only drawback of this standard was the need to use a different solvent for the standard and the dendrimers, but the difference in solvent was accounted for during the calculation of the quantum yield. The quantum yield of each dendrimer was calculated using the method of Parker and Rees[16]. The equation used was:

$$\Phi_{unk} = \frac{A_{stand}\Phi_{stand}F_{unk}\eta_{unk}^2}{A_{unk}F_{stand}\eta_{stand}^2} \tag{3.3}$$

where A is the absorbance, F is the area under the fluorescence spectrum, Φ is the quantum yield, and η is the refractive index of the solvent. The absorbances of the unknown and the standard should both be approximately the same in order to minimize error. The quantum yield was calculated at four different absorbance levels and then the average of the values was reported.

The collected fluorescence data was worked up through a series of steps in order to extract the quantum yield of each sample. The data collected on the fluorimeter was transferred to Microsoft Excel®. In Excel® the blank spectra were normalized to each sample spectra. Normalization was completed using the peak corresponding to $2\lambda_{ex}$ and was accomplished by finding the maximum y-value in the blank spectrum and its corresponding x-value. The y-value for each sample spectra corresponding to the x-value from the blank spectrum was found and then divided by the maximum y-value from the blank spectrum. This gives the normalization factor, which the intensities of the blank spectra were multiplied by to give normalized blank spectra. This results in a specific

normalized blank spectrum for each sample spectrum. The normalized blank spectrum was then subtracted from the appropriate sample spectrum. The normalized sample spectrum was then transferred to KaleidaGraph®. The resulting area under the resulting fluorescence curve was then calculated using a macro included in the program. The macro does not include any negative y-values in the calculation of the area.

Chapter 3 References

1. Turro, N.J., et al., *Photoinduced Electron-Transfer Reactions to Probe the Structure of Starburst Dendrimers.* Macromolecules, 1990. **23**: p. 910-912.
2. Frechet, J.M.J. and A. Adronov, *Light-Harvesting Dendrimers.* Chemical Communications, 2000: p. 1701-1710.
3. Frechet, J.M.J. and M. Kawa, *Self-assembled lanthanide-cored dendrimer complexes: Enhancement of the luminescence properties of lanthanide ions through site-isolation and antenna effects.* Chemistry of Materials, 1998. **10**(1): p. 286-296.
4. Balzani, V., et al., *Supramolecular Dendrimers with a [Ru(bpy)3]2+ Core and Naphthyl Peripheral Units.* New Journal of Chemistry, 1999: p. 63-69.
5. Vogtle, F., et al., *Dendrimers with a photoactive and redox-active Ru(bpy)(3) (2+)-type core: Photophysical properties, electrochemical behaviour, and excited-state electron-transfer reactions.* Journal of the American Chemical Society, 1999. **121**(26): p. 6290-6298.
6. Aida, T., T. Sato, and D.L. Jiang, *A Blue-Luminescent Dendritic Rod: Poly(phenyleneethynylene Within a Light-Harvesting Dendritic Envelope.* Journal of the American Chemical Society, 1999. **121**: p. 10658-10659.
7. Kaifer, A.E., et al., *Dendrimers Functionalized with a Single Fluorescent Dansyl Group Attached "Off Center": Synthesis and Photophysical Studies.* Journal of the American Chemical Society, 2000. **122**(26): p. 6139-6144.
8. Castellano, F.N., X. Zhou, and D.S. Tyson, *First Generation Light-Harvesting Dendrimers with a [Ru(bpy)3]2+ Core and Aryl Ether Ligands Functionalized with Coumarin 450.* Angewandte Chemie International Edition in English, 2000. **39**(23): p. 4301-4305.
9. Frechet, J.M.J., S.L. Gilat, and A. Adronov, *Light Harvesting and Energy Transfer in Novel Convergently Constructed Dendrimers.* Angewandte Chemie International Edition in English, 1999. **38**(10): p. 1422-1427.
10. Moore, J.S., P. Bharathi, and C. Devadoss, *Energy Transfer in Dendritic Macromolecules: Molecular Size Effects and the Role of an Energy Gradient.* Journal of the American Chemical Society, 1996. **118**: p. 9635-9644.
11. Kopelman, R., et al., *Dendrimer photoantenna supermolecules: Energetic funnels, exciton hopping, and unusual excimer formation.* Abstracts of Papers of the American Chemical Society, 1999. **218**: p. 17-PHYS.
12. Gray, T.G., et al., *Highly emissive hexanuclear rhenium(III) clusters containing the cubic cores Re6S8 (2+) and Re6Se8 (2+).* Inorganic Chemistry, 1999. **38**(26): p. 5932-+.
13. Gray, T.G., et al., *Spectroscopic and Photophysical Properties of Hexanuclear Rhenium (III) Chalcogenide Cluster.* Journal of the American Chemical Society, 2003. **125**: p. 4755-4770.
14. Frechet, J.M.J., et al., *Effects of dendrimer Generation on Site Isolation of Core Moieties: Electrochemical and Fluorescence Quenching Studies with Metalloporphyrin Core Dendrimers.* Chemical Materials, 1998. **10**: p. 30-38.

15. Gorman, C.B. and M. Sheepwash, *Personal Communication*. 2003.
16. Parker, C.A. and W.T. Rees, *Correction of Fluorescence Spectra and Measurement of Fluorescence Quantum Efficiency.* 1960: p. 587-600.

Chapter 4 : Electrochemical Investigation

Introduction

It is necessary to understand the electrochemical properties of rhenium-selenide core dendrimers in solution before solid-state investigations. Previous studies have exhibited the electrochemical properties of rhenium-selenide core molecules[1-3]. In this study the effect of the attached dendrons and generational effects were studied. The results of these studies as well as solvent effects are presented in this chapter.

Results and Discussion

CV

Original cyclic voltammetry experiments were designed to reproduce results of previous group members[4]. The electrochemical solutions were made with high analyte and counterion concentrations in propylene carbonate. Propylene carbonate was not considered a good electrochemical solvent for solution electrochemistry, but it was chosen because of poor solubility in dimethylformamaide. Analyte concentrations of 4mM to 8mM were investigated, with 300mM counterion. The high concentrations of analyte and counterion were a function of the poor conductivity of propylene carbonate. Poor solubility in dimethylformamide may have been due to the use of impure samples[5].

Analysis of rhenium-selenide core dendrimers began with the investigation of a precursor, $[Re_6Se_8(CH_3CN)_6]^{2+}$. Solutions of 2mM and 3mM were compared to determine the ideal concentration. The only difference between solutions of 2mM and 3mM was the passage of more current in the 3mM solution, but both solutions offered

enough data for analysis. In order to conserve material, 2mM solutions of $[Re_6Se_8(CH_3CN)_6]^{2+}$ were used.

Once the electrochemical window for $[Re_6Se_8(CH_3CN)_6]^{2+}$ was established, $[Re_6Se_8(G0)_6]^{2+}$ was investigated using similar potential windows. Solubility was an issue at 2mM and 1mM concentrations. Solutions allowed to sit overnight resulted in the majority of the solid dissolving for both concentrations. However, small amounts of a white solid were still observed in both solutions. Samples were filtered though a syringe filter prior to electrochemical analysis. $[Re_6Se_8(G1)_6]^{2+}$ exhibited similar solubility problems at 1mM. A solution allowed to sit still had copious amounts of undissolved solid remaining in the vial. Preliminary cyclic voltammetry was completed, but the concentration of the sample was unknown and therefore little data could be collected.

A plot of the peak currents versus scan rate in propylene carbonate for G0 dendrimer, shown in **Fig IV.1**, is linear showing that the analyte behaved as a freely diffusing molecule.

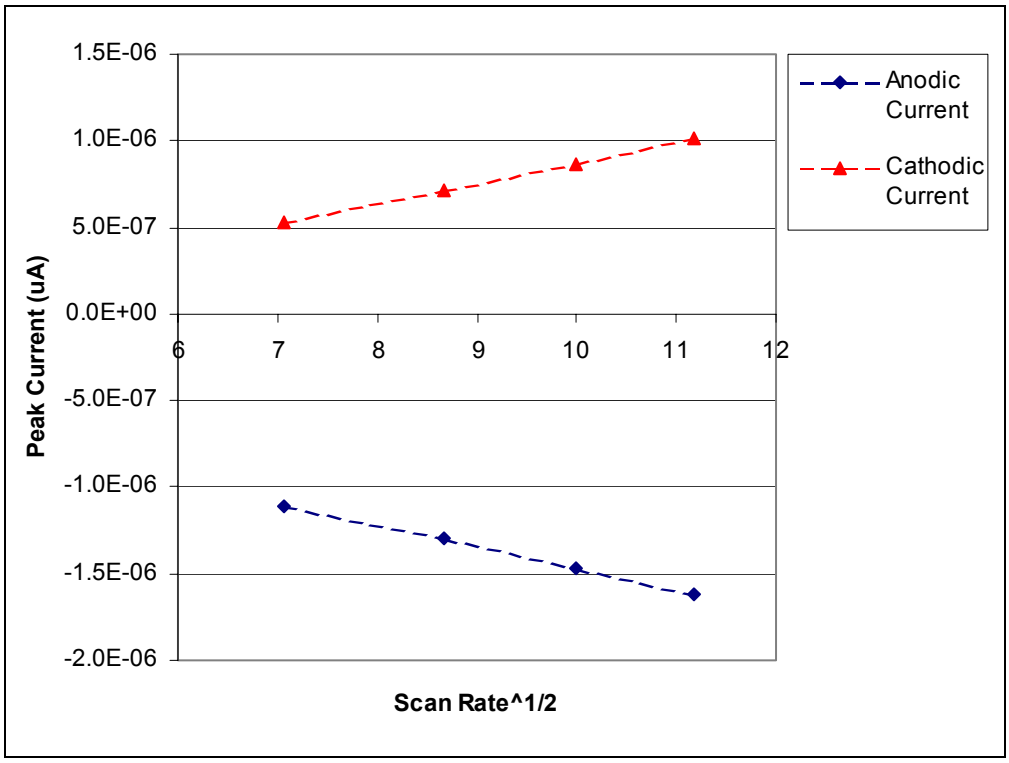


Figure 4.1: G0 dendrimer acting as a freely diffusing molecule

Plots of the cyclic voltammetry of $[Re_6Se_8(CH_3CN)_6]^{2+}$ and $[Re_6Se_8(G0)_6]^{2+}$ are shown in **Figure IV.2**. The $E_{1/2}$ and ΔE values are shown in **Table IV.1**. There was a shift in the redox potential towards more negative potentials from $[Re_6Se_8(CH_3CN)_6]^{2+}$ to $[Re_6Se_8(G0)_6]^{2+}$. The shift to a more negative potential was most likely due to the addition of the electron donating methoxy groups. There appeared to be little difference between G0 and G1 based on the location of the reduction peak in the G1 voltammagram.

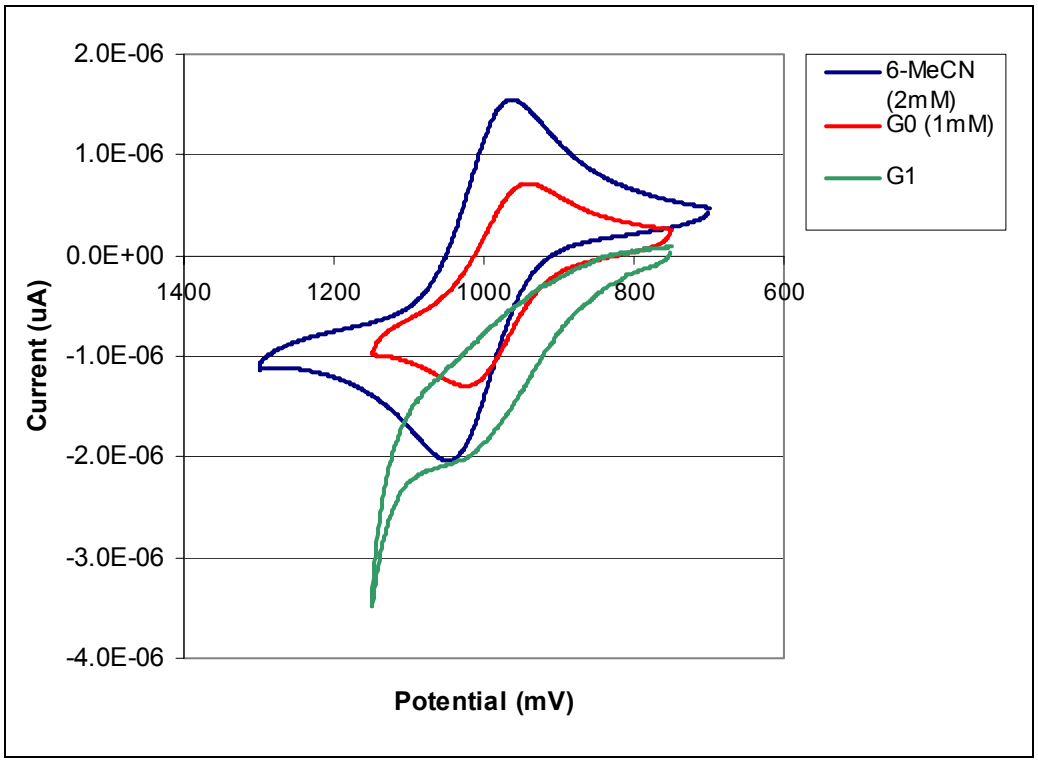


Figure 4.2: Cyclic voltammery of $[Re_6Se_8(CH_3CN)_6]^{2+}$, $[Re_6Se_8(G0)_6]^{2+}$, and $[Re_6Se_8(G1)_6]^{2+}$ in propylene carbonate, scan rates were 100mV/sec

Table 4.1: Electrochemical values of $[Re_6Se_8(CH_3CN)_6]^{2+}$ and $[Re_6Se_8(G0)_6]^{2+}$

Analyte	$E_{1/2}$(mV)	D_0(cm^2/sec)	K_{et}	R_H(Å)
$[Re_6Se_8(CH_3CN)_6]^{2+}$	1008	1.84×10^{-6}	5.28×10^{-3}	29.36
$[Re_6Se_8(G0)_6]^{2+}$	986	4.30×10^{-6}	3.49×10^{-2}	7.50

Attempts at electrochemistry in dimethylformamide using previously prepared dendrimers exhibited quasi-reversible behavior with $E_{1/2}$ between 700-800mV for all three dendrimer generations. However, following changes made to the dendrimer synthesis this data could not be reproduced. This redox potential did not agree with the ~1000mV redox potential in propylene carbonate and also did not agree with the data fro the freshly prepared dendrimers. Another problem with cyclic voltammetry in

dimethylformamide was the proximity of the solvent window to the redox potential of the $[Re_6Se_8]^{2+}$ core. The solvent window for dimethylformamide was found to be approximately 1100mV and was about 100mV away from the redox potential of $[Re_6Se_8(CH_3CN)_6]^{2+}$. This caused difficulty in setting the window such that the data collected would not be skewed by current due to the solvent window being reached.

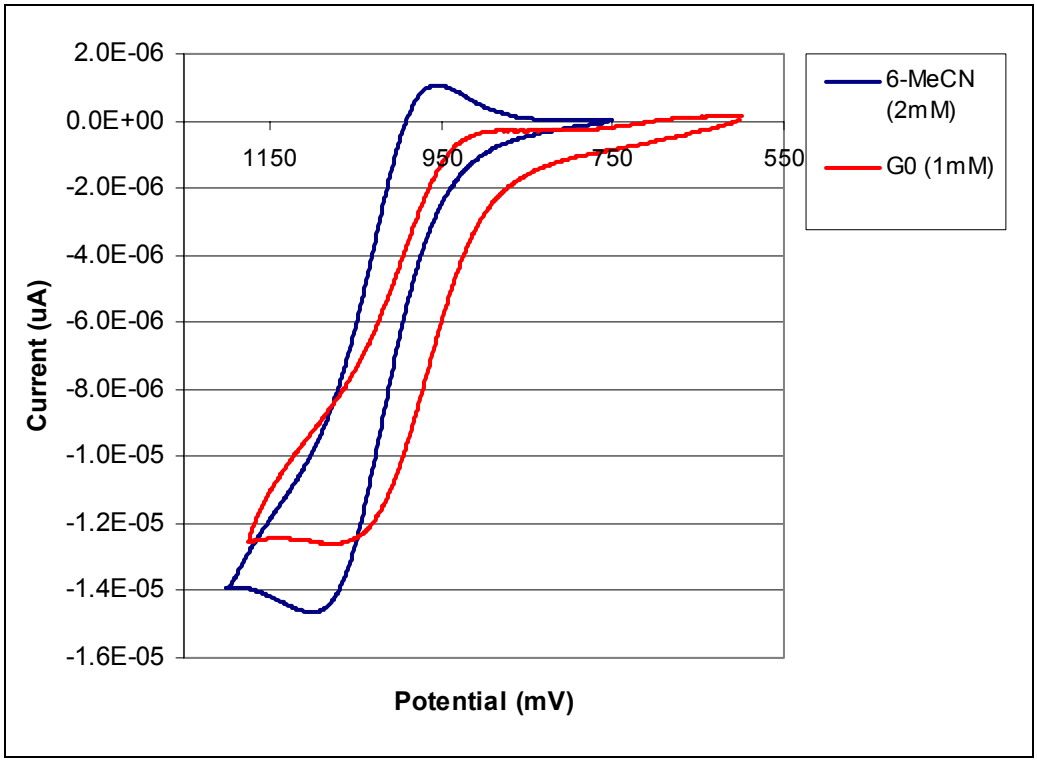


Figure 4.3: Cyclic voltammetry of $[Re_6Se_8(CH_3CN)_6]^{2+}$ and $[Re_6Se_8(G0)_6]^{2+}$ in dimethylformamide with 100mV/sec scan rate

Chronoamperometry

The Cottrell window was reestablished and was found to differ from previous investigations[4]. The diffusion coefficients are listed in **Table IV.1**. The small diffusion coefficient for $[Re_6Se_8(CH_3CN)_6]^{2+}$ may have been due to aggregation and the

resulting calculated radius was much larger then expected. The distance between the rhenium atoms in other rhenium-selenide core molecules is only 2.6Å and therefore a radius of 29.4Å appeared incorrect. The diffusion coefficient of the G1 dendrimer was not investigated because of the uncertainty of the concentration.

OYSW

Oysteryoung squarewave voltammetry was used to determine the rate of electron transfer. The different rates of transfer are shown in **Table IV.1**. The rate of electron transfer for $[Re_6Se_8(CH_3CN)_6]^{2+}$ was not considered correct due to the low diffusion coefficient value. The problems with $[Re_6Se_8(CH_3CN)_6]^{2+}$ also did not allow for comparisons of the rate of electron transfer with $[Re_6Se_8(G0)_6]^{2+}$ dendrimer. The rate of electron transfer for $[Re_6Se_8(G1)_6]^{2+}$ was not calculated because of the concentration problems. The oysteryoung squarewave voltammetry of both $[Re_6Se_8(CH_3CN)_6]^{2+}$ and $[Re_6Se_8(G0)_6]^{2+}$ showed areas of inconsistency from 700mV to 800mV. This area was nearly linear and differed from the rest of the data. This became a concern during data fitting because it was necessary to remove this area, but there was a concern that too much data would be removed and hence alpha values would be incorrect.

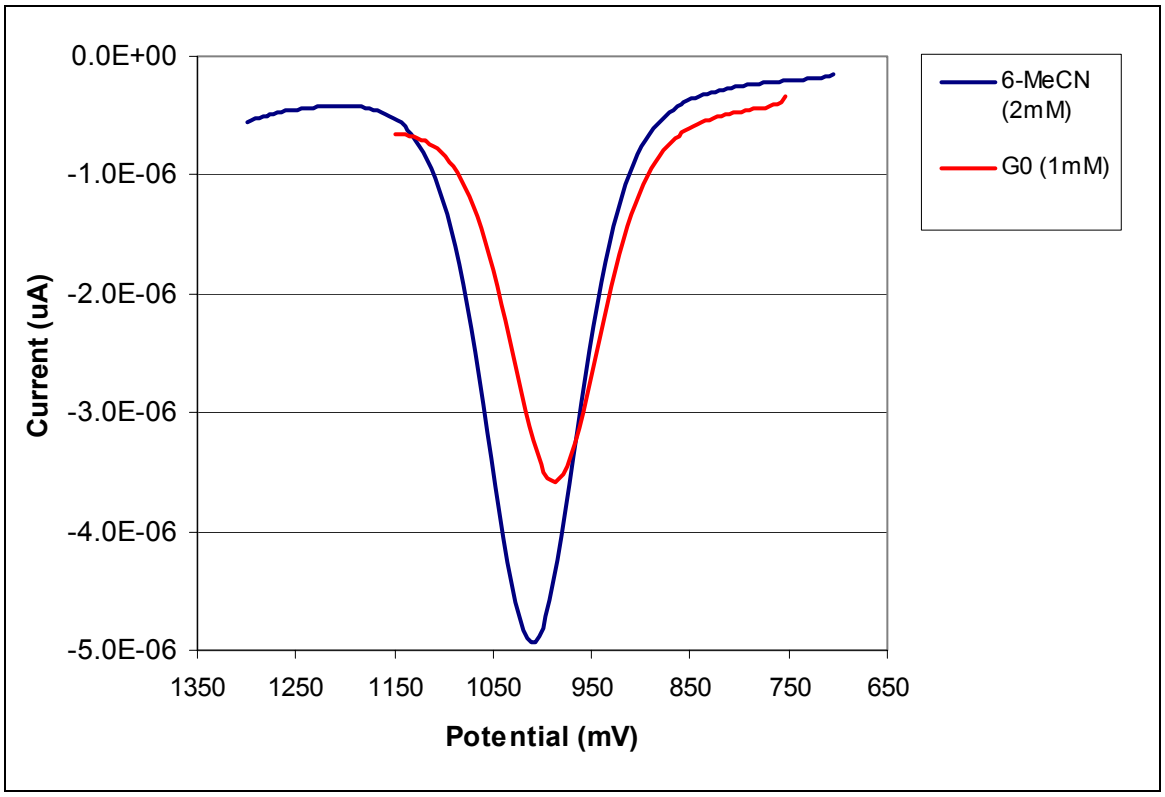


Figure 4.4: Oysteryoung squarewave voltammetry of $[Re_6Se_8(CH_3CN)_6]^{2+}$ and $[Re_6Se_8(G0)_6]^{2+}$ in propylene carbonate

The electrochemical investigations of rhenium-selenide core dendrimers exhibited poor redox kinetics in the solvents investigated. Poor solubility and poor reversibility were causes for concern and led to premature termination of electrochemical characterization. There are plans to investigate electrochemical characterization in methylene chloride, but more dendrimer must be synthesized. The proposed work in methylene chloride requires the use of a special electrochemical cell designed to keep the sample air-free during all measurements. Care must be taken to ensure that air is removed from the electrolyte salt prior to solvent addition and from the analyte prior to electrolyte solution addition.

Experimental

General Considerations. Electrochemical experiments were completed using two different Bioanalytical Systems CV-50W Voltammeric Analyzers. The electrochemical cells used consisted of a three-electrode system: a platinum-disc working electrode (geometric area of 0.0201cm^2), a platinum auxiliary electrode, and a custom $Ag/AgNO_3$ reference electrode. The reference electrode consisted of a silver wire submerged in 10mM $AgNO_3$ and 100mM supporting electrolyte, tetraethylammonium tetrafluoroborate ($TEABF_4$), in acetonitrile[6]. Experiments in dimethylformamide and propylene carbonate were carried out in a nitrogen-filled Vacuum Atmospheres controlled atmosphere box at room temperature. Solutions in dimethylformaide were prepared with 2mM analyte and 100mM $TEABF_4$. Solutions in propylene carbonate were prepared with 1mM analyte and 300mM $TBABF_4$.

Platinum disc working electrodes were polished according to proper technique, conditioned, and then referenced to $[Fe_4S_4(S\text{-}\mathbf{G1Flex})_4][Bu_4N]_2$[7]. Electrode surfaces were also inspected under microscope to ensure that there were no defects to the area surrounding the platinum disc. Once all electrodes yielded data[8] within an acceptable range, analyte samples were analyzed using varying scan rates or pulse widths and with two different electrodes to ensure reproducible data and no fouling of the electrode.

Cyclic Voltammetry. Experiments were conducted using sweep rates of 50, 75, 100, and 125 mV/sec for all analytes displaying quasireversible electrochemical behavior. Scan rates were varied by going from 50 to 125, then back down from 125 to 50. One

more random scan rate was chosen to ensure that the data collected did not show any unexpected patterns.

Analysis of the cyclic voltammetry data was completed using the Nicholson analysis. The Nicholson analysis uses peak separation to calculate the electron transfer kinetics and includes a parameter, ψ, which relates the peak separation to the electron transfer kinetics. The Nicholson analysis is best used for ΔE values between 80 and 120 mV. At ΔE values of less then 80 mV, ψ increases exponentially and at ΔE values greater then 120 mV, there is almost no change in ψ.

Chronoamperometry. Chronoamperometry was preformed on all molecules exhibiting quasireversible cyclic voltammagrams. Irreversible systems were not subjected to chronoamperometry because experimental conditions would destroy the analyte solution. The Cottrell region was determined and pulse widths of 1250, 1500, and 1750 were used to determine the diffusion coefficient. The diffusion coefficient was calculated using the following:

$$i_p = \frac{nFADC}{\Pi^{1/2}} \qquad \text{(IV.1)}$$

Which rearranges to:

$$D = \frac{i_p \Pi^{1/2}}{nFAC} \qquad \text{(IV.2)}$$

where i_p is the peak current, n is the number of electrons transferred, A is the area of the electrode, C is the concentration, and F is Faraday's constant.

Osteryoung Square Wave Voltammetry. Oysteryoung square wave voltammetry was conducted using a 4mV step height, 25mV sweep width amplitude, and frequencies of 5, 10, 15, 20, and 25Hz. The frequencies were varied up, down, one random point, and then repeated with a second electrode. The difference current was then iteratively fit, attempting to achieve $\alpha = 0.5$ using FSQPLT software[9]. The iterative fitting resulted in obtaining $E_{1/2}$ and log $(\kappa_0/(t_d)^{1/2})$). The electron transfer rate constant was then calculated using:

$$\log \kappa/(t_d)^{1/2} = \log \left(\left(k_o / D_o^{1/2}\right) t_d^{1/2}\right) \qquad \text{(IV.3)}$$

where t_d is the experimental pulse period, D_o is the molecular diffusion coefficient, and κ is the reduced rate constant.

Chapter 4 References

1. Batail, P., et al., *Chemistry of Hexanuclear Rhenium Chalcohalide Clusters.* Chemical Reviews, 2001. **101**: p. 2037-2066.
2. Holm, R.H. and Z.P. Zheng, *Cluster condensation by thermolysis: Synthesis of a rhomb- linked Re12Se16 dicluster and factors relevant to the formation of the Re24Se32 tetracluster.* Inorganic Chemistry, 1997. **36**(23): p. 5173-5178.
3. Zheng, Z., B.K. Roland, and C. Carter, *Routes to Metallodendrimers of the [Re6(μ3-Se)8]2+ Core-Containing Clusters.* Journal of the American Chemical Society, 2002. **124**: p. 6234-6235.
4. Smith, J.C., *Laboratory Notebook, JCSIV*.
5. Gorman, C.B., *Personal Communication*. 2001.
6. *BioAnalytic Systems website*.
7. Smith, J.C., *Structure-property Relationships for Alternatively Stiff and Flexible Redox-Active Core Dendrimers of the Type, [Fe4S4(S-Dend)4]2-*, in *Chemistry*. 1999, North Carolina State University: Raleigh.
8. Chasse, T.L., *Gorman group electrochemical investigation procedure*. 2003.
9. O'Dea, J., *FSQPLT*.